Catalytic applications of Transition Metal Complexes with NHC ligands

M.Sc. Research Thesis

CH 800

by **Saurabh Molpha**Roll No. 2303131023



DEPARTMENT OF CHEMISTRY INDIAN INSTITUTE OF TECHNOLOGY INDORE MAY 2025

Catalytic applications of Transition Metal Complexes with NHC ligands A THESIS

Submitted in partial fulfillment of the requirements for the award of the degree

of

Master of Science

by

Saurabh Molpha

Roll no. 2303131023



DEPARTMENT OF CHEMISTRY INDIAN INSTITUTE OF TECHNOLOGY INDORE MAY 2025



INDIAN INSTITUTE OF TECHNOLOGY INDORE

CANDIDATE'S DECLARATION

I hereby certify that the work which is being presented in the thesis entitled "Catalytic applications of transition metal complexes with NHC ligands," in the partial fulfilment of the requirements for the award of the degree of MASTER of SCIENCE and submitted to the DEPARTMENT of CHEMISTRY, Indian Institute of Technology Indore, is an authentic record of my work carried out during the period July 2024 to May 2025 under the supervision of **Dr. Amrendra K. Singh,** Department of Chemistry, Indian Institute of Technology Indore. The matter presented in this thesis has not been submitted by me for the award of any other degree of this or any other institute.

Saurabh Molpha

20105/25

Signature of the Student

This is to certify that the above statement made by the candidate is correct to the best of my/our knowledge.

Dr. Amrendra K. Singh

Signature of the M.Sc. Thesis Supervisor

Saurabh Molpha has successfully given his M. Sc oral Examination held on 14/05/2025.

Signature of supervisor of M. Sc Thesis

Date: 20/5/2025

.....

ACKNOWLEDGEMENTS

Initially, I express my gratitude towards my thesis supervisor, **Dr. Amrendra Kumar Singh**, for providing me with valuable guidance, suggestions, and supervision, as well as for offering constant encouragement throughout my research work. Additionally, I express my gratitude to the members of my PSPCcommitteemembers, **Dr. Abhinav Raghuvanshi** and **Prof. Shaikh M. Mobin** for their significant contributions and assistance. I am thankful to the **Department of Chemistry** at IIT Indore for providing me with the opportunity to undertake this research endeavor. Special acknowledgment goes to **Prof. Tushar Kanti Mukherjee**, the Head of the Department of Chemistry at the Indian Institute of Technology Indore, for his support and encouragement. I feel incredibly obligated to take this chance to express my gratitude to the teachers and SIC personnel at IIT Indore for their support and cooperation throughout this dissertation project.

I would like to extend my gratitude to my laboratory colleagues Ms. Ekta Yadav, Mr. Shambhu Nath, Ms. Achena Saha, Mr. Ashu Singh, Mr. Vishal Jaiswal, and Mr. Naveen Kumar, who consistently provided me with valuable insights and unwavering support in pursuit of the project's objectives. The information that you generously imparted to me was greatly motivating, not only for the present undertaking but also for the broader realm of communication practice. I want to express my gratitude to my brothers, who have always supported me and never let me down throughout my life. Finally, I'd like to express my deepest appreciation to my parents for all their support and encouragement during the duration of this endeavor.

Saurabh Molpha M. Sc. 2nd year Roll No. 2303131023 Department of Chemistry

Dedicated to my parents and my mentor.

ABSTRACT

Transition metal complexes bearing protic-NHC (N-heterocyclic carbene) ligands have attracted significant attention due to their unique structural and electronic properties. However, their catalytic potential remains relatively underexplored. This work presents and discusses the catalytic applications of ruthenium complexes featuring protic-NHC ligands. Specifically, we report the synthesis and characterization of pincer ligand-based ruthenium complexes incorporating halide derivatives, iodo and chloro as the sixth coordinating ligand. The Ru (II) CNN complexes have been characterized by LC-MS, multinuclear spectroscopy (¹H, ¹³C), and SCXRD. Spectroscopic **NMR** investigations, including UV-Visible and fluorescence spectroscopy, were performed, along with electrochemical studies using cyclic voltammetry (CV) and differential pulse voltammetry (DPV). The catalytic activity of CNN-based metal complexes towards amine double-dehydrogenation, hydration of nitriles, and water oxidation catalysis has been explored.

TABLE OF CONTENTS PAGE NO. LIST OF FIGURES XIII-XVII LIST OF SCHEMES XIX XXI **ACRONYMS** NOMENCLATURE XXIII **CHAPTER 1:** 1 INTRODUCTION 1.1 Aim of the project 1 1.2 General Introduction 1 2 1.3 N-Heterocyclic carbene 3 1.4 Ru metal Precursor 5 1.5 Hydration of Nitriles 6 1.6 Amine doubledehydrogenation 1.7 Water Oxidation 7 **CHAPTER 2:** 10 **EXPERIMENTAL SECTION** 2.1 General information 10 2.2 Chemicals and reagents 10 2.3 Instrumentation 10

3.1 Synthesis of Ligand Precursor	16
3.2 Synthesis of Metal Precursor	17
3.3 Synthesis of Complex Ru-1 & Ru-2	20
3.4 Description of Crystal Structure (Ru-1)	21
3.5 Characterization of Ligand L1	23
3.6 Characterization of Ligand L2	24
3.7 Characterization of Ligand L3	25
3.8 Characterization of Precursor P1	26
3.9 Characterization of Precursor P2	26
3.10 Characterization of Precursor P3	28
3.11 Characterization of Precursor P4	29
3.12 Characterization of Precursor P5	29
3.13 Characterization of Precursor P6	30
3.14 Characterization of Precursor P7	30
3.15 Characterization of Complex Ru-1	32
3.16 Characterization of Complex Ru-2	33
3.17 Photoluminescent Studies	35
3.18 Emission Spectra	37
3.19 Electrochemical Studies of Ruthenium Complexes	38
3.20 Catalytic Applications	40
CHAPTER 4: CONCLUSION AND FUTURE SCOPE	58
4.1 Future Scope	58
4.2 References	59

LIST OF FIGURES

- Fig. 1: First stable N-Heterocyclic carbene
- Fig. 2: N-heterocyclic Carbenes
- **Fig. 3:** Some selected active ruthenium catalysts for the hydration of nitriles
- Fig. 4: Examples of drug molecules
- Fig. 5: SCXRD of Ru-1 complex
- **Fig. 6:** ¹H NMR of Ligand L1
- Fig. 7: ¹³C NMR of Ligand L1
- Fig. 8: ¹H NMR of Ligand L2
- Fig. 9: ¹³C NMR of Ligand L2
- Fig. 10: HRMS of Ligand L3
- **Fig. 11:** ¹H NMR of Ligand L3
- Fig. 12: ¹³C NMR of Ligand L3
- Fig. 13: LC-MS of Precursor P1
- Fig. 14: ¹H NMR of Precursor P2
- Fig.15: ¹³C NMR of Precursor P2
- Fig. 16: LC-MS of Precursor P2
- Fig. 17: ¹H NMR of Precursor P3
- Fig. 18: ¹³C NMR of Precursor P3
- Fig. 19: LC-MS of Precursor P4
- Fig. 20: LC-MS of Precursor P5
- Fig. 21: ¹H NMR of Precursor P6
- Fig. 22: LC-MS of Precursor P6
- Fig. 23: ¹H NMR of Precursor P7
- Fig. 24: ¹³C NMR of Precursor P7
- Fig. 25: LC-MS of Complex Ru-1
- Fig. 26: ¹H NMR of Complex Ru-1
- Fig. 27: ¹³C NMR of Complex Ru-1

- Fig. 28: ¹H NMR of Complex Ru-2
- Fig. 29: ¹³C NMR of Complex Ru-2
- Fig. 30: LC-MS of Complex Ru-2
- **Fig. 31:** UV-vis spectra of Complex Ru-1 recorded in CH₃OH at room temperature
- **Fig. 32:** UV-vis spectra of Complex Ru-2 recorded in CH₃OH at room temperature
- **Fig. 33:** Emission spectra of Complex Ru-1 recorded in CH₃CN at room temperature
- **Fig. 34:** Emission spectra of Complex Ru-2 recorded in CH₃CN at room temperature
- **Fig. 35:** Cyclic Voltammograms of Ru-1 in 0.1 TBAPF₆ recorded in CH₃CN at scan rates between 50 mV/s to 1000 mV/s.
- **Fig. 36:** Cyclic Voltammograms of Ru-2 in 0.1 TBAPF₆ recorded in CH₃CN at scan rates between 50 mV/s to 1000 mV/s.
- Fig. 37. GC-MS spectrum for entry 1 of Table 1
- Fig. 38. GC-MS spectrum for entry 2 of Table 1
- Fig. 39. GC-MS spectrum for entry 3 of Table 1
- **Fig. 40.** GC-MS spectrum for entry 4 of Table 1
- Fig. 41. GC-MS spectrum for entry 5 of Table 1
- Fig. 42. GC-MS spectrum for entry 6 of Table 1
- Fig. 43. GC-MS spectrum for entry 7 of Table 1
- Fig. 44. GC-MS spectrum for entry 2 of Table 2
- Fig. 45. GC-MS spectrum for entry 3 of Table 2
- **Fig. 46:** Cyclic voltammogram of complex Ru-1 recorded in CH₃CN using 0.1 M TBAPF₆ as the supporting electrolyte.
- **Fig. 47.** DPV of complex Ru-1 recorded in CH₃CN using 0.1 M TBAPF₆ as the supporting electrolyte.
- Fig. 48. Cyclic voltammogram of complex Ru-2 recorded in

CH₃CN using 0.1 M TBAPF₆ as the supporting electrolyte.

Fig. 49: DPV of complex Ru-1 recorded in CH₃CN using 0.1 M TBAPF₆ as the supporting electrolyte.

Fig. 50: ¹H NMR spectrum (500 MHz) of [**Ru-2**] in DMSO-d₆ after addition of base.

Fig. 51: ¹H NMR spectrum (500 MHz) of [**Ru-2**] in DMSO-d₆ after H₂ bubbling.

List of Schemes

Scheme 1. Conversion of Benzonitrile to Benzamide

Scheme 2. Conversion of Benzylamine to Benzonitrile

Scheme 3. Splitting of water

Scheme 4. Synthesis of Ligand precursor L3

Scheme 5. Synthesis of Metal Precursor P1

Scheme 6. Synthesis of Metal Precursor P2 & P3

Scheme 7. Synthesis of Metal Precursor P4 & P5

Scheme 8. Synthesis of Metal Precursor P6 & P7

Scheme 9. Synthesis of Complex Ru-1

Scheme 10. Synthesis of Complex Ru-2

Scheme 11. Conversion of Benzylamine to Benzonitrile

Scheme 12. Conversion of Benzonitrile to Benzamide

Scheme 13. Oxygen evolution experiment in 0.1M HNO₃

ACRONYMS

ACN Acetonitrile

CAN Ceric ammonium nitrate

CDCl₃ Chloroform-d CHCl₃ Chloroform

DCM Dichloromethane
DMSO Dimethyl sulfoxide

ESI Electron spray ionization

HRMS High-resolution mass spectrometry

K₂CO₃ Potassium carbonate

LC-MS Liquid chromatography-mass spectrometry

MeOH Methanol

Na₂SO₄ Sodium sulfate

NMR Nuclear magnetic resonance

NH₄Cl Ammonium chloride

TLC Thin layer chromatography

NOMENCLATURE

°C Degree Celsius

h hour

Hz Hertz

M Molar

mL Millilitre

mg Milligrams

MHz megahertz

mmol millimole

nm Nanometer

ppm Parts per million

CHAPTER 1

INTRODUCTION

1.1 Aim of the project:

The aim of this thesis is to synthesize and investigate iodo and chlorobased CNN ruthenium pincer complexes, with a particular focus on their potential for various catalytic applications. Additionally, this study aims to explore their catalytic activities in a range of applications, including nitrile hydration, hydrogenation, hydrosilylation, and N-methylation of amine. The strong σ-donating ability of the NHC ligand contributes to the formation of electron-rich complexes, making them promising candidates for the activation of small molecules in key transformations such as ammonia oxidation, water oxidation, and CO₂ reduction. Through these investigations, this work seeks to advance the understanding of the structure-activity relationships of these complexes and their broader catalytic applications. We look forward to further exploring its capabilities and advancing our understanding in this field.

1.2 General Introduction:

Pincer ligands play an important role in various areas of transition metal catalysis. They are widely used in reactions such as cross-coupling, polymerization, Diels-Alder reactions, and most notably, in hydrogenation and dehydrogenation reactions.¹ Pincer ligands, characterized by their unique tridentate coordination to the metal center, significantly contribute to improving the efficiency and selectivity of various catalytic processes.² Pyridine dicarbene pincer ligands, which incorporate N-heterocyclic carbenes (NHCs), are especially favored for their ability to increase electron density at the ruthenium center, thereby enhancing the metal's reactivity in catalytic transformations.³

The use of ruthenium pincer complexes as catalysts has gained significant attention in recent years due to their ability to control reactivity, stability, and selectivity in various chemical reactions and catalyst designs. Ruthenium complexes exhibit several advantageous

properties, such as efficient electron transfer, strong coordination ability with heteroatoms, low redox potentials, Lewis acidic behavior, and distinctive reactivity of metal species and intermediates, including oxo-metal complexes, metallacycles, and carbenes.⁴ Ruthenium pincer complexes have attracted considerable attention as catalysts due to their accessibility in multiple stable oxidation states and their ability to adopt various coordination geometries, such as square pyramidal, trigonal bipyramidal, and octahedral.³

Transition metal complexes containing N-heterocyclic carbenes (NHCs) have gained significant attention in organometallic chemistry and catalysis. This is mainly because NHCs offer a wide range of electronic and structural properties and can form highly stable metal-ligand bonds.⁵ Due to their unique properties and broad range of applications, NHC-based metal complexes are considered a promising area of research with strong potential for future advancements. In particular, Ruthenium NHC complexes containing the NHC moiety show enhanced reactivity, making them suitable for various catalytic processes. This increased reactivity makes ruthenium complexes attractive for a wide range of catalytic applications.⁶

The stability of NHC-based transition metal complexes allows for their efficient use as catalysts, enabling the development of new synthetic methodologies and the synthesis of complex organic molecules.^{7,8}

1.3 N-Heterocyclic carbene (NHC):

N-Heterocyclic carbenes (NHCs) are a versatile class of cyclic carbenes containing at least two heteroatoms, typically nitrogen. Their unique electronic properties and structural flexibility have made them indispensable in modern organometallic chemistry and catalysis. NHCs are characterized by their strong σ -donor and weak π -acceptor properties, which contribute to their stability and ability to form strong metal-ligand bonds. The ease of preparation

, thermal stability, and tunability of NHCs have led to their widespread use as alternatives to phosphine ligands in various catalytic systems.

Fig. 1: First stable N-Heterocyclic carbene. 11

N-Heterocyclic carbene (NHC) chemistry began in 1968 with the pioneering work of Ofele¹² and Wanzlick¹³, who focused on metal coordination compounds derived from azolium salts.

A major breakthrough occurred in 1991 when Arduengo successfully isolated a free carbene, renewing interest in the field. ¹⁴ Since then, NHC ligands have been widely applied in various catalytic reactions such as Heck, Sonogashira, and Suzuki cross-couplings, hydrogenation, C–H activation, and olefin metathesis. The high stability of NHC-based transition metal complexes enables efficient catalytic performance, which has led to the development of new synthetic strategies and the preparation of complex organic molecules. ⁸ This progress has sparked renewed attention in NHC chemistry, especially because of the promising role of these ligands in organometallic catalysis.

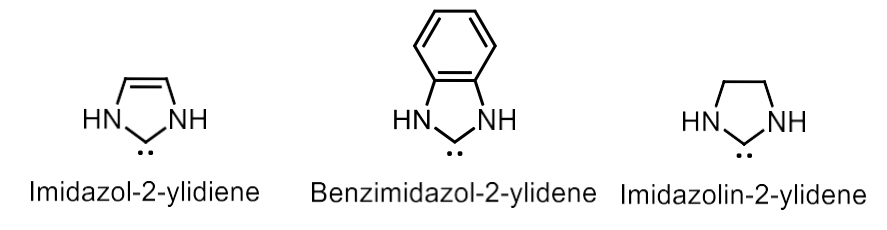


Fig. 2: N-heterocyclic Carbenes

1.4 Ru-metal Precursor:

Ruthenium(II) complexes, particularly those incorporating NHC ligands, have emerged as a powerful class of organometallic compounds with diverse applications. ¹⁵ The synergy between ruthenium and NHC ligands has resulted in catalysts with exceptional performance in a wide range of transformations. Some key features and applications of Ru-NHC complexes include the following:

- a. Catalytic versatility: Ru-NHC complexes excel in numerous reactions, including olefin metathesis, transfer hydrogenation, C-H activation, and cross-coupling reactions. 16
- b. Tunable properties: The modular nature of NHC ligands allows for fine-tuning of steric and electronic properties, enabling the development of tailored catalysts for specific applications.¹⁷
- c. Medicinal applications: Ru-NHC complexes have shown promise as potential anticancer agents, leveraging the unique properties of ruthenium in biological systems.¹⁸
- d. Renewable energy: These complexes have found applications in dye-sensitized solar cells (DSSCs), contributing to advancements in sustainable energy technologies.^{19,20}
- e. Stability and activity: Ru-NHC complexes often exhibit enhanced thermal stability and catalytic activity compared to their phosphine counterparts.

Ruthenium pincer complexes have gained significant attention, representing approximately 13% of recent research in the pincer complex field.²¹ These complexes, characterized by tridentate pincer ligands, offer additional stability and control over the metal centre's reactivity. Ru-pincer complexes have shown exceptional performance in various catalytic processes, including:

- i. Hydrogenation and dehydrogenation reactions
- ii. C-C and C-heteroatom bond formation
- iii. CO₂ activation and utilization
- iv. Water oxidation catalysis

The combination of NHC ligands with pincer architectures in ruthenium complexes has led to the development of highly efficient and robust catalytic systems. These advanced catalysts continue to push the boundaries of organic synthesis and sustainable chemistry, offering new possibilities for challenging transformations and green chemical processes.²²

Ru-CNN pincer complexes have shown significant promise in catalysis, but several challenges persist. These include limited stability under reaction conditions, which can lead to

decomposition or deactivation over time. Achieving high selectivity remains difficult, as these complexes may catalyze multiple reactions, resulting in undesired by-products. Ligand degradation, particularly under harsh conditions, further hampers efficiency. Fine-tuning the reactivity for specific reactions is also a challenge, as precise control over the ligand's electronic and steric properties is required. So, to overcome these challenges, several robust pincer complexes have been prepared over time.

1.5 Hydration of Nitriles

Due to their unique structural properties and reactivity, amides are extensively employed as intermediates in the design and synthesis of pharmaceuticals, functional materials, and high-performance polymers. ^{23,24} Among the various synthetic strategies developed for amide formation, the condensation of carboxylic acids with amines is regarded as one of the most straightforward and widely adopted approaches. 25,26 Among the numerous strategies explored, the hydration of nitriles has emerged as a convenient and sustainable approach due to its environmentally friendly nature and absence of toxic byproducts. ^{24,26} Conventional methods for nitrile hydration often involve harsh conditions, typically requiring strongly acidic or alkaline media, which pose significant challenges in terms of sustainability and environmental compatibility. ^{27,28} A wide range of transition metal-based catalysts have been developed for nitrile hydration, promoting the direct nucleophilic addition of water to the nitrile bond and thereby facilitating the efficient formation of amides. ^{29–31} Ruthenium-based catalysts have shown considerable promise in nitrile hydration, enabling high selectivity and efficiency under mild reaction environments. 32 Cadierno and colleagues investigated a ruthenium-based catalyst for the hydration of nitriles, demonstrating its effectiveness even at low catalyst loading (1 mol%) in an aqueous medium. ³³ Recently, Otten ²⁴ and Gupta ³² reported the use of ruthenium catalysts for nitrile hydration under mild reaction conditions, utilizing pincer and tridentate ligands. A selection of active ruthenium catalysts for this reaction under mild

conditions is presented below (Fig. 1).

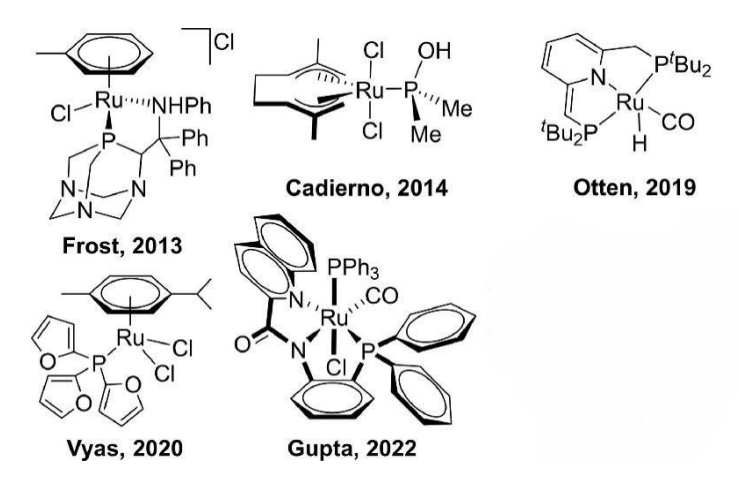


Fig. 3: Some selected active ruthenium catalysts for the hydration of nitriles.

$$\begin{array}{c|c}
 & & & & \\
 & & & \\
 & & & \\
 & & & \\
 & & & \\
 & & & \\
 & & & \\
 & & & \\
 & & & \\
 & & & \\
 & & & \\
 & & & \\
 & & & \\
 & & & \\
 & & & \\
 & & & \\
 & & & \\
 & & & \\
 & & & \\
 & & & \\
 & & & \\
 & & & \\
 & & & \\
 & & & \\
 & & & \\
 & & & \\
 & & & \\
 & & & \\
 & & & \\
 & & & \\
 & & & \\
 & & & \\
 & & & \\
 & & & \\
 & & & \\
 & & & \\
 & & & \\
 & & & \\
 & & & \\
 & & & \\
 & & & \\
 & & & \\
 & & & \\
 & & & \\
 & & & \\
 & & & \\
 & & & \\
 & & & \\
 & & & \\
 & & & \\
 & & & \\
 & & & \\
 & & & \\
 & & & \\
 & & & \\
 & & & \\
 & & & \\
 & & & \\
 & & & \\
 & & & \\
 & & & \\
 & & & \\
 & & & \\
 & & & \\
 & & & \\
 & & & \\
 & & & \\
 & & & \\
 & & & \\
 & & & \\
 & & & \\
 & & & \\
 & & & \\
 & & & \\
 & & & \\
 & & & \\
 & & & \\
 & & & \\
 & & & \\
 & & & \\
 & & & \\
 & & & \\
 & & & \\
 & & & \\
 & & & \\
 & & & \\
 & & & \\
 & & & \\
 & & & \\
 & & & \\
 & & & \\
 & & & \\
 & & & \\
 & & & \\
 & & & \\
 & & & \\
 & & & \\
 & & & \\
 & & & \\
 & & & \\
 & & & \\
 & & & \\
 & & & \\
 & & & \\
 & & & \\
 & & & \\
 & & & \\
 & & & \\
 & & & \\
 & & & \\
 & & & \\
 & & & \\
 & & & \\
 & & & \\
 & & & \\
 & & & \\
 & & & \\
 & & & \\
 & & & \\
 & & & \\
 & & & \\
 & & & \\
 & & & \\
 & & & \\
 & & & \\
 & & & \\
 & & & \\
 & & & \\
 & & & \\
 & & & \\
 & & & \\
 & & & \\
 & & & \\
 & & & \\
 & & & \\
 & & & \\
 & & & \\
 & & & \\
 & & & \\
 & & & \\
 & & & \\
 & & & \\
 & & & \\
 & & & \\
 & & & \\
 & & & \\
 & & & \\
 & & & \\
 & & & \\
 & & & \\
 & & & \\
 & & & \\
 & & & \\
 & & & \\
 & & & \\
 & & & \\
 & & & \\
 & & & \\
 & & & \\
 & & & \\
 & & & \\
 & & & \\
 & & & \\
 & & & \\
 & & & \\
 & & & \\
 & & & \\
 & & & \\
 & & & \\
 & & & \\
 & & & \\
 & & & \\
 & & & \\
 & & & \\
 & & & \\
 & & & \\
 & & & \\
 & & & \\
 & & & \\
 & & & \\
 & & & \\
 & & & \\
 & & & \\
 & & & \\
 & & & \\
 & & & \\
 & & & \\
 & & & \\
 & & & \\
 & & & \\
 & & & \\
 & & & \\
 & & & \\
 & & & \\
 & & & \\
 & & & \\
 & & & \\
 & & & \\
 & & & \\
 & & & \\
 & & & \\
 & & & \\
 & & & \\
 & & & \\
 & & & \\
 & & & \\
 & & & \\
 & & & \\
 & & & \\
 & & & \\
 & & & \\
 & & & \\
 & & & \\
 & & & \\
 & & & \\
 & & & \\
 & & & \\
 & & & \\
 & & & \\
 & & & \\
 & & & \\
 & & & \\
 & & & \\
 & & & \\
 & & & \\
 & & & \\$$

Scheme 1: Conversion of Benzonitrile to Benzamide

1.6 Amine double-dehydrogenation:

In the realm of significant organic compounds, aryl nitriles hold a vital position as they are commonly present in natural products, pharmaceuticals, agrochemicals, materials, and dyes.³⁴ The significant role of aryl nitriles in both biology and chemistry has continually driven the advancement of novel synthesis methods.

Nitriles are frequently found in bioactive molecules, natural products, and essential compounds for various industrial applications.³⁵ In pharmaceuticals, many pharmaceutical drugs contain nitrile (cyanide) groups, such as Milrinone,³⁶ Febuxostat,³⁷ and Etravirine,³⁸ which are essential for treating diabetes, arthritis, and AIDS, respectively.

Fig. 4: Examples of drug molecules that contain cyano groups

Traditional methods for synthesizing nitriles often encounter problems such as inefficient use of atoms, reliance on toxic reagents, and limited selectivity. Common techniques, including ammoxidation, Sandmeyer reaction, oxidation with hypervalent iodine compounds, and transition-metal-catalyzed oxidations, are often hindered by issues like restricted reactivity, poor resource utilization, the requirement for mild reaction conditions, and limited compatibility with various functional groups.³⁹

The transition-metal catalyzed process, in which double dehydrogenation of primary amines is done, presents an alternative, atom-economical strategy that eliminates the stoichiometric oxidants. This reaction occurs under acceptor-less conditions. 40 This process is facilitated by the removal of H₂ gas as the sole byproduct. However, the studies on the double dehydrogenation of primary amines are limited, and most available catalysts tend to yield low results or require the addition of exogenous bases and/or hydrogen acceptors.41,42

Scheme 2: Conversion of Benzylamine to Benzonitrile

1.7 Water Oxidation:

Water oxidation is vital for energy storage, particularly in the realm of

renewable energy. As we move toward sustainable solutions, achieving efficient energy storage and hydrogen production becomes increasingly important.⁴³ Our promising approach to energy storage through water splitting focuses on the oxidation of water to produce oxygen. Consequently, the development of an efficient water oxidation catalyst is essential for the success of this strategy. A variety of metal-based catalysts, such as those containing Ruthenium, Iridium, and Cobalt, have been investigated for their potential in facilitating water oxidation.^{44,45}

Efficient water oxidation catalysts play a vital role in advancing energy storage systems that rely on water splitting. The hydrogen fuel generated through this method serves as a clean energy source for fuel cells, offering a sustainable replacement for conventional fossil fuels. Additionally, the oxygen byproduct can be leveraged in industrial applications, including chemical synthesis and renewable fuel manufacturing. As a critical component of sustainable energy infrastructure, optimizing water oxidation efficiency remains a priority, driving ongoing research efforts to develop robust, cost-effective catalysts such as iron-based complexes and transition metal oxides.

$$2H_2O \longrightarrow 4H^+ + 4e^- + O_2$$

Scheme 3: Splitting of water

Inspired by the natural process of photosynthesis, many researchers have been working on creating artificial systems that can replicate this process to split water into oxygen and hydrogen.⁴⁸ In 1982, a team of researchers led by Meyer Made made a revolutionary breakthrough known as the "Blue dimer".⁴⁹ In 2005, Thummel and his team achieved a major breakthrough by developing the first-ever mononuclear ruthenium water oxidation catalyst.⁵⁰

The catalyst has been widely utilized in sustainable energy applications, particularly for converting solar energy into chemical energy by splitting water molecules to generate oxygen and hydrogen.⁵¹ Its development has paved the way for researchers to

investigate more efficient and cost-effective methods of producing clean energy. In 2019, Ahlquist and colleagues offered important evidence highlighting the role of a dangling carboxylate group in facilitating proton-coupled electron transfer (PCET) reactions. By employing an intramolecular proton relay, they provided deeper insights into the fundamental mechanisms involved. ⁵²

In 2012, Son and his research group achieved a significant breakthrough by developing a highly efficient water oxidation catalyst [Ru(bda)(pic)2].⁵³

CHAPTER 2

EXPERIMENTAL SECTION

2.1 General information:

All of the chemicals and solvents used in this study were purchased from commercially accessible sources. No purification was done before their use. However, hexane and ethyl acetate were distilled before usage. The experiments were conducted in a nitrogen-filled Schlenk line. The results were monitored using Merck 60 F254 precoated silica gel plates for thin-layer chromatography (TLC). To purify the products, column chromatography with silica gel (100-200 mesh) was employed.

2.2 Chemicals and Reagents:

Without any additional purification, all of the reagents and solvents utilized in this experiment were obtained from commercial sources. These chemicals include Benzimidazole (SRL, 99%), imidazole (SRL, 99%), 2,6- dibromo pyridine (Alfa Aesar, 98%), 2-bromo pyridine (Spectrochem, 99%), potassium carbonate (SRL, 99.5%), sodium bicarbonate (SRL, 99.5%), ruthenium trichloride trihydrate (SRL), potassium hydroxide (Emplura, 85%), Sodium hydroxide (Emplura, 84%), Methyl iodide (Spectrochem, 99%), Isopropyl bromide (Spectrochem, 99%), 1-Methlyimidazole (Spectrochem, 99%).

2.3 Instrumentation:

The ADVANCE III 400 and 500 MHz Ascend Bruker BioSpin machines were used to record NMR spectra at ambient temperature. For mass spectrometric analyses, the Bruker-Daltonics micro to-Q II mass spectrometer was utilized.

2.4 **SYNTHESIS OF LIGANDS:**

2.4.1 Synthesis of Ligand L1:

Experimental procedure:

2,6-dibromopyridine (2.3684 g, 0.01 mol), Benzimidazole (1.1813 g, 0.01 mol), CuI (0.3804 g, 0.002 mol), K₂CO₃ (3.8697 g, 0.028 mol), TMEDA (0.7 mL), and dry DMSO (20 mL) were added to a two-neck round flask and treated for 45 minutes at 85 °C in the microwave. After completion, the mixture was extracted with brine solution and DCM. The compound was dried over anhydrous Na₂SO₄, and the crude residue was purified through silica gel (60-120 mesh) column chromatography using hexane/ethyl acetate (70:30) as eluent to obtain a product. The crude product 77% (0.8556 g) was obtained, and the characterization for ¹H NMR and ¹³C NMR data, which shows the confirmation of the ligand. ¹H NMR (500 MHz, CDCl₃, 25 °C δ 8.57 (s, 1H), 8.08 (d, J =8.3 Hz, 1H), 7.85 (s, 0H), 7.74 (t, J = 7.8 Hz, 1H), 7.53 (d, J = 7.9 Hz, 1H), 7.47 (d, J = 7.7 Hz, 1H), 7.39 (dtd, J = 19.5, 7.3, 1.3 Hz, 2H), 7.27 (s, 0H), 2.03 (s, 1H). ${}^{13}C{}^{1}H$ NMR (126 MHz, CDCl₃, 25 °C) δ 149.69, 144.71, 141.25, 141.02 (d, J = 7.5 Hz), 131.88, 125.89, 123.86, 120.87, 113.03, 112.28, 77.44 – 76.89 (m).

2.4.2 Synthesis of Ligand L2:

p-toluidine (2.1432 g, 0.020 mol) and 2-bromopyridine (3.1598 g, 0.020 mol) were added to a pressure tube and heated in an oil bath at 160 °C for 24h. Upon completion of the reaction, the mixture was extracted with a saturated Na₂CO₃ solution. The resulting yellow precipitate was separated by filtration. The solid was then washed with DCM, and the combined organic layers were concentrated under reduced pressure using a rotary evaporator to reduce DCM. Hexane was subsequently added to the residue to induce further precipitation, and the mixture was allowed to stand undisturbed for two days to facilitate complete crystallization. After this period, the precipitated product was isolated by filtration and analyzed by thin-layer chromatography (TLC) to confirm its identity and purity. Yield: 79% (2.94 g) and the characterization for ¹H NMR (500 MHz, CDCl₃, 25 °C) δ 8.18 – 8.14 (m, 1H), 7.44 (ddd, J = 8.8, 7.1, 1.9 Hz, 1H), 7.25 (s, 0H), 7.21 – 7.12 (m, 4H), 6.82 (d, J = 8.6 Hz, 1H), 6.68 (ddd, J = 7.2, 5.0, 0.9 Hz, 1H),2.32 (s, 3H). ¹³C{¹H} NMR (126 MHz, CDCl₃, 25 °C) δ 156.76, 148.41,

137.84 (d, *J* = 11.1 Hz), 132.90, 129.95, 121.42, 114.63, 107.78, 20.93.

2.4.3 Synthesis of Ligand L3:

An oven-dried 100 mL 2-neck R.B. flask, fitted with a reflux condenser was charged with L1 (1.777 g, 0.00965 mol), L2 (2.0346 g, 0.00742 mol), Pd(dba)₂ (0.17088 g, 0.000297 mol), dppf (0.16465 g, 0.000297 mol), KO^tBu (1.00121 g, 0.008907 mol, 1.2 equiv.) and anhydrous toluene (20 mL) under inert atmosphere. The flask was lowered into an oil bath and heated to reflux for 24h at 110 °C. After cooling the reaction mixture to room temperature, ethyl acetate (20 mL) was added and stirred for 30 minutes, resulting in the formation of a red precipitate. The mixture was filtered through Celite to remove the precipitate, and the filtrate was evaporated under reduced pressure using a rotary evaporator to obtain a brown solid. The crude product was then purified by column chromatography on silica gel (60-120 mesh) using ethyl acetate/hexane (70:30) as the eluent, yielding 2.19 g of a light brown solid (78% yield). The characterization for **HRMS** (ESI) m/z calculated for $C_{24}H_{19}N_5[M+H]^+$ 378.1715, found 378.1713 and ¹**H NMR** (500 MHz, CDCl₃, 25 °C) δ 8.41 (dd, J = 4.6, 2.1 Hz, 1H), 8.39 (s, 1H), 7.76 (d, J = 8.1 Hz, 1H), 7.69 (t, J = 8.0 Hz, 1H), 7.60 (ddd, J = 8.2, 7.3, 2.0 Hz, 1H), 7.56 (d, J = 8.2 Hz, 1H), 7.29 -7.19 (m, 3H), 7.12 - 6.99 (m, 4H), 2.43 (s, 2H). ¹³C{¹H} NMR $(126 \text{ MHz}, \text{CDCl}_3, 25 \text{ °C}) \delta 157.62 \text{ (d, } J = 29.5 \text{ Hz)}, 148.53 \text{ (d, } J = 29.5 \text{ Hz)}$ 3.8 Hz), 144.53, 141.80, 141.05, 139.92, 137.89, 136.57, 132.15, 130.76, 128.34, 123.80, 123.06, 120.27, 119.03, 118.18, 113.97, 111.98, 105.52, 21.25.

2.5 **SYNTHESIS OF COMPLEXES:**

2.5.1 Synthesis of Precursor P1:

2-bromopyridine (1.5799 g, 0.010 mol) and 1*H*-imidazole (2.042 g, 0.030 mol) were charged in a pressure tube at 190 °C in a silicon oil bath for 18h. After completion, the mixture was extracted with DCM and water. After the rotary evaporator, a clear solution was kept in a vacuum. The obtained product was 87% (1.2675 g), and the characterization for **LC-MS** (ESI) m/z calculated for $C_8H_7N_3$ [M+H] ⁺ 146.0713, found 146.0859.

2.5.2 Synthesis of precursor P2:

2-(1*H*-imidazol-1-yl)pyridine (3.266 g, 0.0221 mol) and Iodomethane (2.75 mL, 0.0442 mol) with toluene (10 mL) were added in a pressure tube at 110 °C in a silicon oil bath for 24h. After completion, the mixture was washed with THF solvent. The Deccan process is used to get the compound. A yellow product obtained 75% (4.8655 g), and the characterization for **LC-MS** (ESI) m/z calculated for C₉H₁₀N₃ [M]⁺ 160.0869, found 160.0871. ¹H NMR (500 MHz, CDCl₃, 25 °C) δ 10.72 (s, 1H), 8.48 (d, 1H), 8.24 (t, 2H), 7.98 (t, 1H), 7.82 (s, 1H), 7.53 (t, 1H), 4.26 (s, 3H). ¹³C{¹H} NMR (126 MHz, CDCl₃, 25 °C) δ 149.25, 145.78, 140.50, 134.83, 125.31, 124.69, 123.70, 119.01, 114.69.

2.5.3 Synthesis of precursor P3:

A Schlenk tube equipped with a magnetic stirring bar was charged with isopropyl iodide (0.01 mol, 1 mL), along with 2-(1*H*-imidazol-1-yl) pyridine (0.01 mol, 1.5 g). Dry toluene (3 mL) was then added to the mixture at room temperature under a nitrogen atmosphere. The reaction mixture was heated in an oil bath at 110 °C for 24 hours. After completion, the precipitate was filtered to afford yellow solids (62.76% yield), respectively. ¹H NMR (CDCl₃, 500 MHz, 25 °C): δ (ppm) 10.80 (s, 1H), 8.36 (d, 1H), 8.36 (dd, 1H), 8.21 (d, 1H), 7.85 (d, 1H), 7.76 (d, 1H), 5.04 (m, 1H), 1.57 (d, 6H); ¹³C{¹H} NMR (CDCl₃, 126 MHz, 25 °C): δ (ppm) 148.71, 145.56, 140.11, 133.12, 124.84, 120.85, 119.04,

114.72, 53.97.

2.5.4 Synthesis of precursor P4:

P2 (0.100 g, 0.000348 mol), Ruthenium (III) Chloride trihydrate (0.09102 g, 0.000034 mol), and THF (5-6 mL) were added in a 50 mL Schlenk tube in a preheated stirrer at 66 °C for 12h under an inert atmosphere, leading to the formation of a brown precipitate. The resulting solid was collected by filtration, washed multiple times with THF, and dried under vacuum. The obtained product was 91.06% (0.122 g), and the characterization for **LC-MS** (ESI) m/z calculated for C₉H₁₂Cl₃N₃ORu [M-Cl] + 349.45, found: 348.93, [M-Cl+H₂O] + 367.45, found: 366.94.

2.5.5 **Synthesis of precursor P5:**

A Schlenk tube equipped with a magnetic stirring bar was charged with P3 (0.00076 mol, 0.241 g), RuCl₃·3H₂O (0.00076 mol, 0.200 g), and THF (2 mL) under a nitrogen atmosphere. The reaction mixture was stirred at reflux temperature (66 °C) for 12 hours, forming a brown precipitate in a dark brown solution. The resulting brown solid was filtered, washed multiple times with THF, and dried under vacuum to afford (61.15% yield), respectively, **LC-MS**: 376.96 [M–Cl] ⁺.

2.5.6 Synthesis of precursor P6:

[Ru^{III}(PyNHC^{Me})(Cl)₃(H₂O)] (0.288.5 g, 0.00075 mol) was dissolved in DMSO (0.5 mL) in an oven-dried Schlenk tube. The reaction mixture was stirred at room temperature (25–28 °C) for 3 days, resulting in the formation of a yellow suspension. The precipitated product was collected by filtration using Whatman filter paper, washed several times with diethyl ether, and dried under vacuum. The purified product was obtained as a yellow solid (0.0808 g, 47% yield). **LC-MS** (ESI) m/z calculated for C₁₁H₁₇ClN₃O₂RuS [M-Cl-DMSO+H₂O] + 391.36 found: 391.97, C₁₃H₂₁N₃O₂RuS₂ [M-2Cl+H] + 416.04 found: 416.00. ¹H NMR (400 MHz, DMSO-d₆, 25 °C) δ 9.47 (d, J = 5.9 Hz, 1H), 8.33 (s,

1H), 7.96 (dd, 2H), 7.50 (s, 1H), 7.32 (t, J = 6.7 Hz, 1H), 4.16 (s, 3H), 2.54 (s).

2.5.7 Synthesis of precursor P7:

[Ru^{III}(PyNHC^{iPr})(Cl)₃(H₂O)] (0.000485 mol, 0.200 g) was dissolved in DMSO (0.5 mL) in an oven-dried Schlenk tube. The reaction mixture was stirred at room temperature (25–28 °C) for 3 days, resulting in the formation of a yellow suspension. The precipitated product was collected by filtration using Whatman filter paper, washed several times with diethyl ether, and dried under vacuum. The purified product was obtained as a yellow solid, 0.228 g (yield: 73.2%). ¹H NMR (400 MHz, DMSO-d₆, 25 °C) δ 9.45 (d, J = 6.0 Hz, 1H), 8.34 (d, 1H), 8.00 (t, J = 7.8 Hz, 1H), 7.94 (d, J = 8.2 Hz, 1H), 7.68 (d, 1H), 7.35 (d, 1H), 6.31–6.05 (m, 1H), 2.54 (s), 1.45 (d, J = 6.8 Hz, 6H). ¹³C NMR (126 MHz, DMSO-d₆, 25 °C) δ 182.83, 155.14, 152.66, 138.67, 120.87, 120.48, 117.43, 110.60, 49.65, 22.08.

2.5.8 Synthesis of complex Ru-1:

An oven-dried Schlenk tube equipped with a magnetic stirring bar was charged with the L3 (0.00008 mol, 0.03113 g), P6 (0.00008 mol, 0.039 g), and NaI (0.005 mol, 0.7494 g) in ethylene glycol (10 mL). The mixture was refluxed under a nitrogen atmosphere for 4 hours in a preheated oil bath stirrer at 200 °C. After completion, the reaction was cooled to room temperature, and an aqueous solution of KPF₆ (0.184 g, 1 mol in 10 mL of water) was added for ion exchange. The mixture was stirred for 2 minutes, leading to the precipitation of the desired complex. The yellow solid was collected by filtration, washed with water, and dried under vacuum. The obtained product was 0.052 g (70% yield). **LC-MS** (ESI) m/z calculated for C₃₃H₂₈N₈IRu [M]⁺ 765.05, found: 765.03.

2.5.9 Synthesis of complex Ru-2:

An oven-dried Schlenk tube equipped with a magnetic stirring bar was charged with the L3 (0.00008 mol, 0.03113 g), P6 (0.00008 mol, 0.039 g), and LiCl (0.005 mol, 0.2119 g) in ethylene glycol (10 mL). The

the mixture was refluxed under a nitrogen atmosphere for 4 hours in a pre-heated oil bath stirrer at 200 °C. After completion, the reaction was cooled to room temperature, and an aqueous solution of KPF₆ (0.184 g, 1 mol in 10 mL of water) was added for ion exchange. The mixture was stirred for 2 minutes, leading to the precipitation of the desired complex. The yellow solid was collected by filtration, washed with water, and dried under vacuum. **LC-MS** (ESI) *m/z* calculated for C₃₃H₂₈N₈ClRu [M]⁺ 673.66, found: 673.11.

CHAPTER 3

RESULT AND DISCUSSION

3.1 Synthesis of Ligand Precursor:

The unsymmetrical NNC pincer ligand 6-(1H-benzimidazol-1-yl)-N-(pyridin-2-yl)-N-(p-tolyl)pyridin-2-amine (L3) was synthesized in three steps, as outlined in Scheme 4. Precursors L1 and L2 were prepared following reported literature procedures.^{54,55} The final ligand L3 was obtained in 66% yield via a Pd-catalyzed Buchwald–Hartwig cross-coupling reaction between L1 and L2.

To the ligand L1, 2,6-dibromopyridine synthesize benzimidazole were initially treated with K₂CO₃, followed by the addition of TMEDA and dry DMSO. The reaction proceeded via an Ullmann coupling pathway. Ligand L1, characterized by ¹H NMR data, claimed the existence of this compound by giving the resonance at δ 8.57 (s) for the carbon group between the nitrogen atoms of the benzimidazole moiety. On the other side, we synthesized ligand L2 by treating p-toluidine with 2bromopyridine, which was confirmed by ¹H and ¹³C NMR by giving the peaks at δ 8.18 (s) for the secondary amine and δ 2.32 (3H) for the methyl group. NNC pincer ligand (L3) confirmed by **HRMS** (ESI) m/z calculated for $C_{24}H_{19}N_5[M+H]^+$ 378.1715, found 378.1713, and ¹H NMR by giving peaks δ 8.39 (s) for the benzimidazole proton of the carbene group, δ 8.41 (d) ortho pyridyl

proton, δ 2.43 (s) for the methyl group. By ¹³C NMR, giving peaks δ 157.74 and 157.51 for the 2 and 6 positions of pyridine, and δ 21.25 for the methyl carbon. (**Scheme 4**).

Scheme 4: Synthesis of Ligand precursor L3

3.2 Synthesis of Metal Precursor P6 and P7:

To synthesize a phosphine-free ruthenium precursor, 2-(1H-imidazol-1-yl) pyridine (P1) was prepared via a neat reaction, and was characterized by **LC-MS** (ESI) m/z calculated for $C_8H_7N_3$ [M+H] $^+$ 146.0713, found 146.0859. (**Scheme 5**) P1 was charged with alkyl (Me and iPr) iodide, followed by toluene at reflux temperature. 1H NMR of P2 confirmed it by giving the resonance at δ 10.72 (s) for the imidazole proton, and δ 4.26 (s) for the imidazole methyl group. Also, from **LC-MS** (ESI) m/z calculated for $C_9H_{10}N_3$ [M] $^+$ 160.0869, found 160.0871. The 1H NMR data for P3 claimed the existence of this compound by giving the resonance δ 10.68 (s) for the carbenic proton and δ 1.78(d) for twelve methyl protons. (**Scheme 6**) The reaction of ligand precursors (P2 & P3) with RuCl₃·3H₂O in a 1:1 ratio in THF at reflux temperature afforded the [Ru^{III}(PyNHC^R)(Cl)₃(H₂O)] complexes P4 and P5.

The successful preparation of P4 and P5 was achieved with the ligand precursor having iodide counterions. No chemical additive, like a base,

was required for the reaction, and no indication of mixed-halide products was observed in the preparation of P4 and P5 (via mass spectrometry of the crude product). LC-MS (ESI) m/z calculated for C₉H₁₂Cl₃N₃ORu [M-Cl] + 349.45, found: 348.93. (**Scheme 7**) The Ru(II)–NHC–DMSO complexes 2a and 2b were synthesized by dissolving the corresponding Ru(III)-NHC complexes 1a and 1b in DMSO. The reaction temperature and time were optimized to afford the desired complexes in good yields. The most favorable conditions for the synthesis were found to be at ambient temperature (25–28 °C) over a duration of three days, as illustrated in Scheme 8. The successful formation of complexes P6 and P7 under these conditions confirmed both the substitution of the coordinated ligand and the reduction of the Ru(III) centers in P4 and P5, facilitated by DMSO. The resulting complexes were isolated as stable solids, resistant to air and moisture, and remained intact under room temperature storage. Despite their stability, P6 and P7 demonstrated poor solubility in most conventional organic solvents, consistent with previously reported Ru(II)–NHC–DMSO complexes.

LC-MS for P6 (ESI) m/z calculated for C₁₁H₁₇ClN₃O₂RuS [M-Cl-DMSO+H₂O] ⁺ 391.36 found: 391.97, C₁₃H₂₁N₃O₂RuS₂ [M-2Cl+H] ⁺ 416.04 found: 416.00. The ¹H NMR data for P7 claimed the existence of this compound by giving the resonance δ 1.45 (d) for the twelve methyl protons. (**Scheme 8**)

$$\begin{array}{|c|c|}
\hline
 & H \\
 & N \\
 & Br \\
 & N \\
 & N \\
 & \hline
 & N \\
 & \hline
 & N \\
 & N$$

Scheme 5: Synthesis of Metal Precursor P1

Scheme 6: Synthesis of Metal Precursor P2 & P3

Scheme 7: Synthesis of Metal Precursor P4 & P5

$$\begin{array}{c|c}
Cl & N \\
H_2O - Ru - (l) & \hline
& 3 days, rt
\end{array} \qquad \begin{array}{c|c}
S & N & N \\
Cl & Ru - (l) & \hline
& 3 days, rt
\end{array} \qquad \begin{array}{c|c}
Cl & Ru - (l) & \hline
& PyIm^R & S = DMSO
\end{array}$$

$$\begin{array}{c|c}
PyIm^R & PyIm^R & R = Me; P6 & \hline
& R = ^iPr; P5 & R = ^iPr; P7
\end{array}$$

Scheme 8: Synthesis of Metal Precursor P6 & P7

3.3 Synthesis of complex Ru-1 and Ru-2:

The synthesis of Ru(II) pNHC complexes is straightforward and readily scalable. The air- and moisture-stable phosphine-free complexes Ru(NNC)(NC^{Me})I]PF₆ and [Ru(NNC)(NC^{Me})Cl]PF₆. The synthesis of Ru(II) pNHC complexes is straightforward and readily scalable. The air- and moisture-stable phosphine-free complexes $Ru(NNC)(NC^{Me})IPF_6$ and $[Ru(NNC)(NC^{Me})Cl]PF_6$ were obtained by reacting the pincer ligand precursor L3 with previously reported ruthenium precursors P6 in ethylene glycol under a nitrogen environment at reflux temperature. The only variation in the reaction conditions was the use of NaI for the synthesis involving $Ru(NNC)(NC^{Me})IPF_6$ and LiCl for the reaction with $[Ru(NNC)(NC^{Me})Cl]PF_6.$

The Ru(II) complexes were extensively studied using spectroscopic techniques multinuclear NMR, as well as analytical approaches such as high-resolution mass spectrometry. Additionally, the solid-state structures of complex (Ru-1) were elucidated using single-crystal X-ray diffraction. **LC-MS** (ESI) m/z calculated for $C_{33}H_{28}N_8IRu$ [M]⁺ 765.05, found: 765.03 (Ru-1).

LC-MS (ESI) m/z calculated for $C_{33}H_{28}ClN_8Ru$ [M] $^+$ 673.11, found: 673.07 (Ru-2).

Scheme 9: Synthesis of precursor Ru-1

Scheme 10: Synthesis of precursor Ru-2

3.4 Description of Crystal Structure [Ru-1]:

The molecular structure of the [Ru-1] complex was analyzed using single-crystal X-ray diffraction. The resulting crystal structure shows a distorted octahedral geometry around the ruthenium center, within the Pbca space group. The ruthenium is bonded to two five-membered metallacycles from the CNN-based pincer ligand, a five-membered CN^{Me} metallacycle, and an iodide ion at the sixth coordination site. The CNN pincer ligand acts as a tridentate chelate, coordinating the ruthenium center in a meridional arrangement.

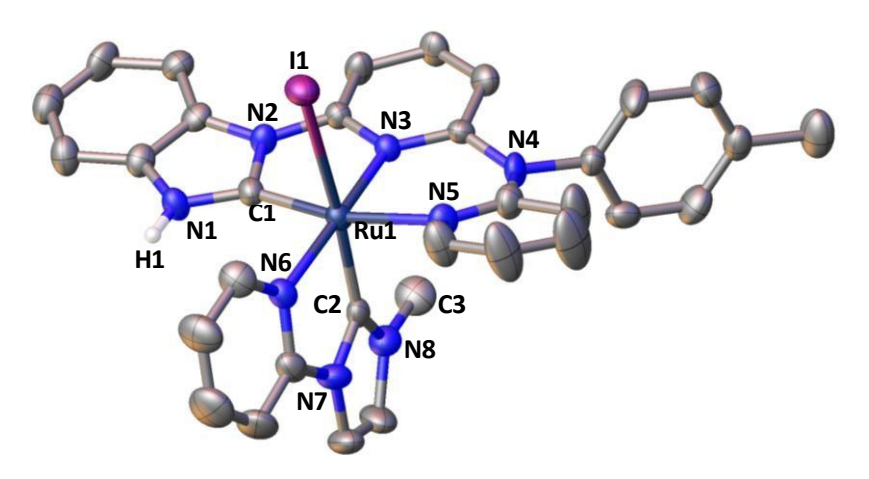


Fig. 5: Single crystal diffracted structure of [Ru-1] complex. All hydrogen atoms (except protic-NH) and one PF₆⁻ counter-anion are omitted for clarity. Selected bond lengths (Å) and angles (°): Ru1-I1, 2.7975(5); Ru1-N6, 2.142(4); Ru1-N3, 2.046(4); Ru1-N6, 2.100(4); Ru1-C1, 1.952(5); Ru1-C2, 1.961(5); N3-Ru1-I1, 88.97(11); N3-Ru1-N5, 88.98(16); N3-Ru-N6, 173.87(15); N5-Ru-I1, 87.42(12); N6-Ru1-I1, 95.11(12); N5-Ru1-N6, 95.79(16); C1-Ru1-I1, 85.85(15); C1-Ru1-N3, 80.21(18); C1-Ru1-N5, 167.33(18); C1-Ru1-N6, 95.49(18); C1-Ru1-C2, 95.0(2); C2-Ru1-I1, 173.29(14); C2-Ru1-N3, 97.74(18);

C2-Ru1-N5, 92.97(18); C2-Ru1-N6, 78.18(18).

The bond length and bond angle formed by ruthenium with both carbene atoms of the pincer, *i.e.*, Ru1–C1 = 1.952(5) Å, Ru1–C2 = 1.961(5) Å, C1–Ru1–C2 = 95.0(2) ° and the bite angle formed by C1–Ru1–N6 = 95.49(18)°. The bidentate ligand CN^{Me} occupies two coordination sites to ruthenium with the bond angle between Ru1–C2 = 1.961(5) Å and bite angle N6–Ru1–C2 = 78.18(18)°.

3.5 Characterization of Ligand L1

3.5.1 NMR spectra of Ligand L1

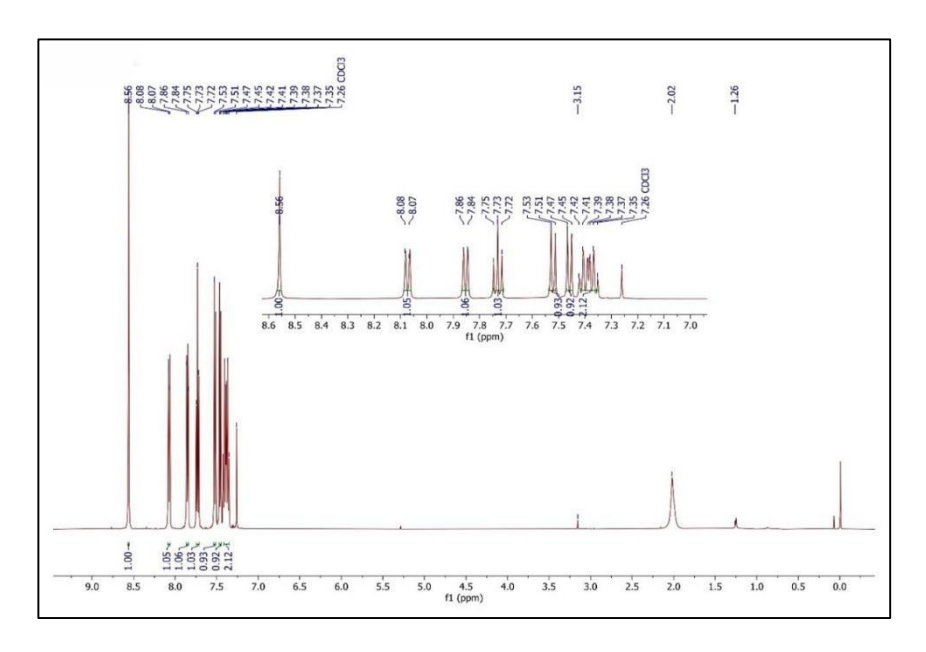


Fig. 6: ¹H NMR of Ligand L1

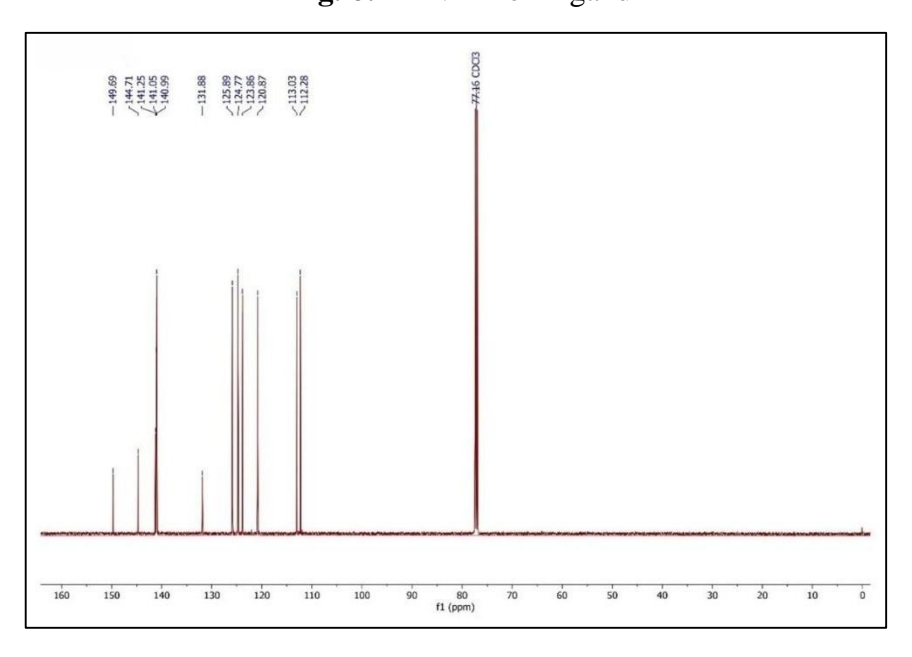


Fig. 7: ¹³C NMR of Ligand L1

3.6 Characterization of Ligand L2

3.6.1 NMR spectra of Ligand L2

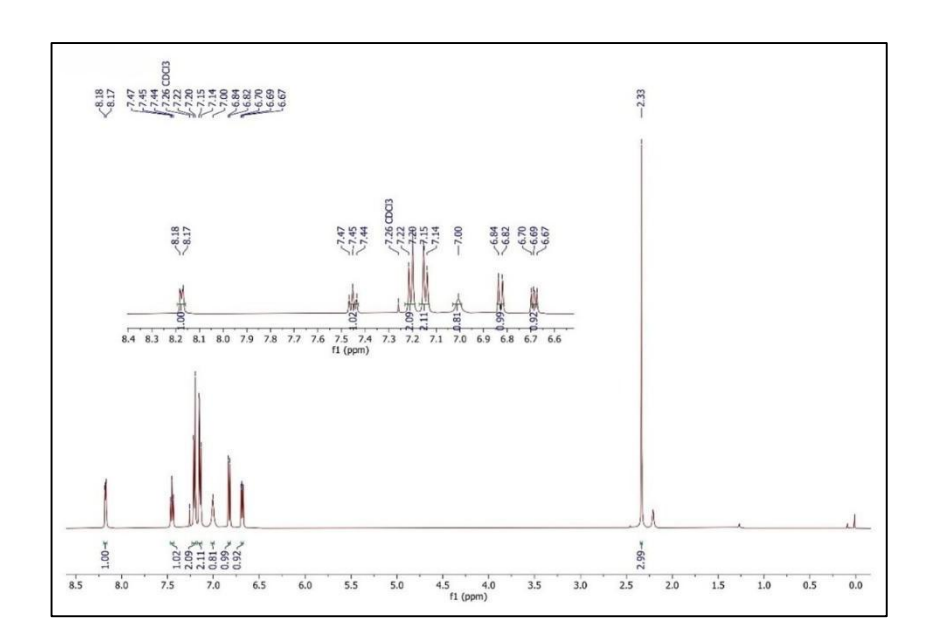


Fig. 8: ¹H NMR of Ligand L2

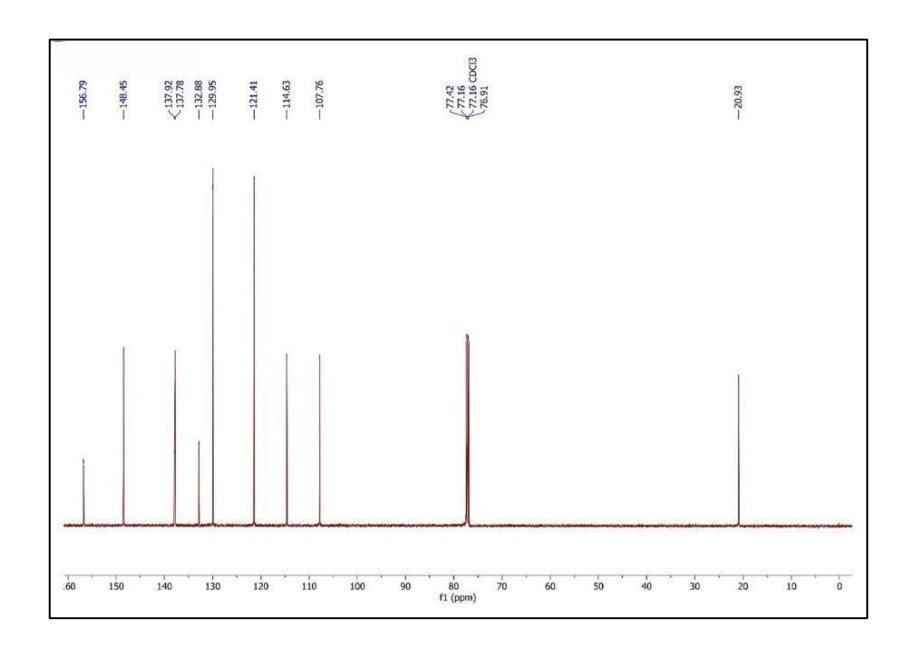


Fig. 9: ${}^{13}C$ { ${}^{1}H$ } NMR of Ligand L2

3.7 Characterization of Ligand L3

3.7.1 HRMS of Ligand **L3**

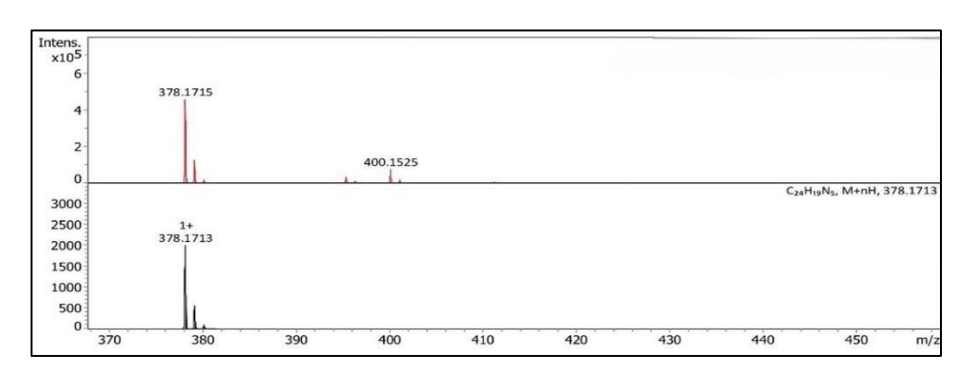


Fig. 10: LC-MS of Ligand L3

3.7.2 NMR spectra of Ligand L3

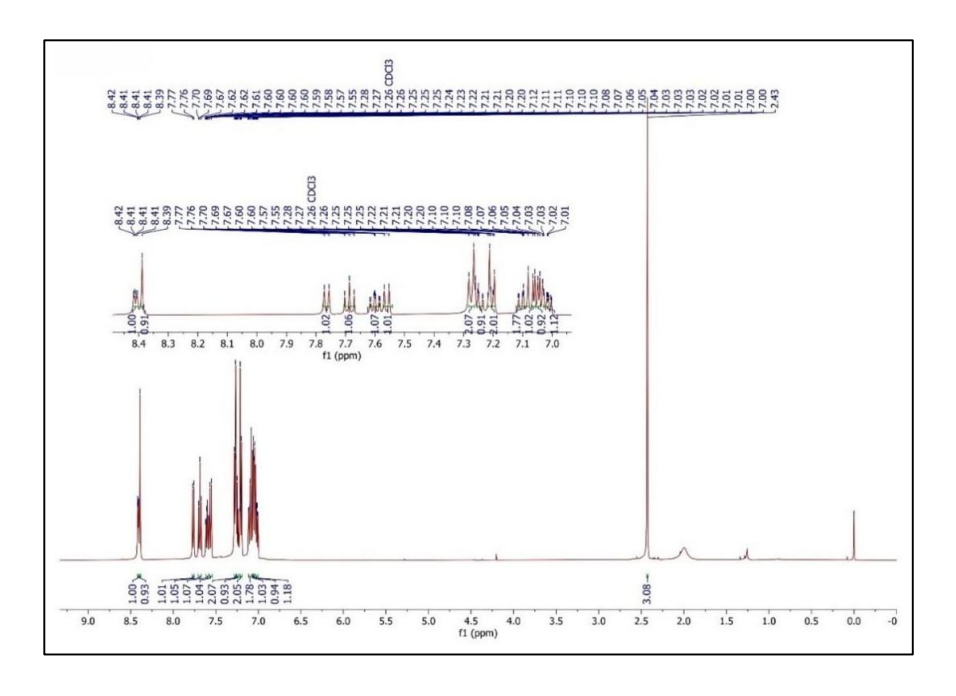


Fig. 11: ¹H NMR of Ligand L3

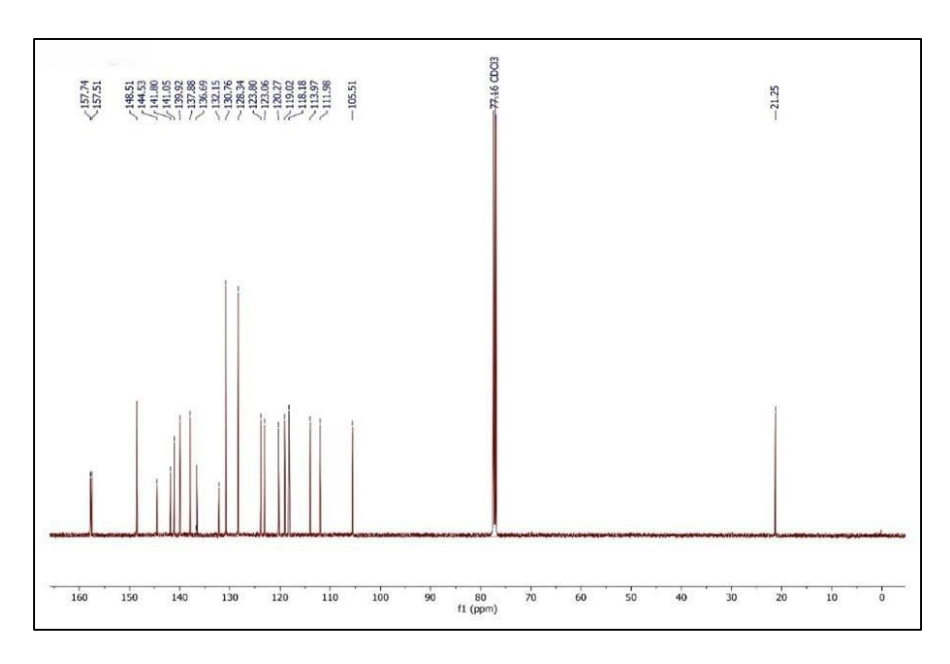


Fig. 12: 13 C $\{^{1}$ H $\}$ NMR of Ligand L3

3.8 Characterization of Precursor P1

3.8.1 LC-MS of Precursor P1

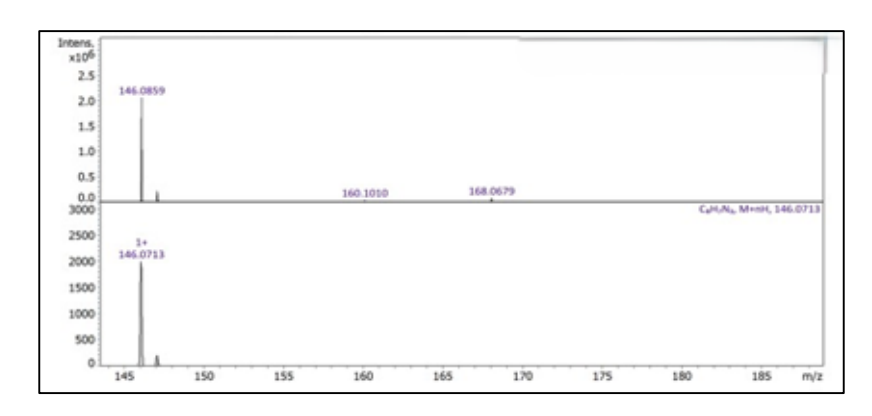


Fig. 13: LC-MS of precursor P1

3.9 Characterization of Precursor P2

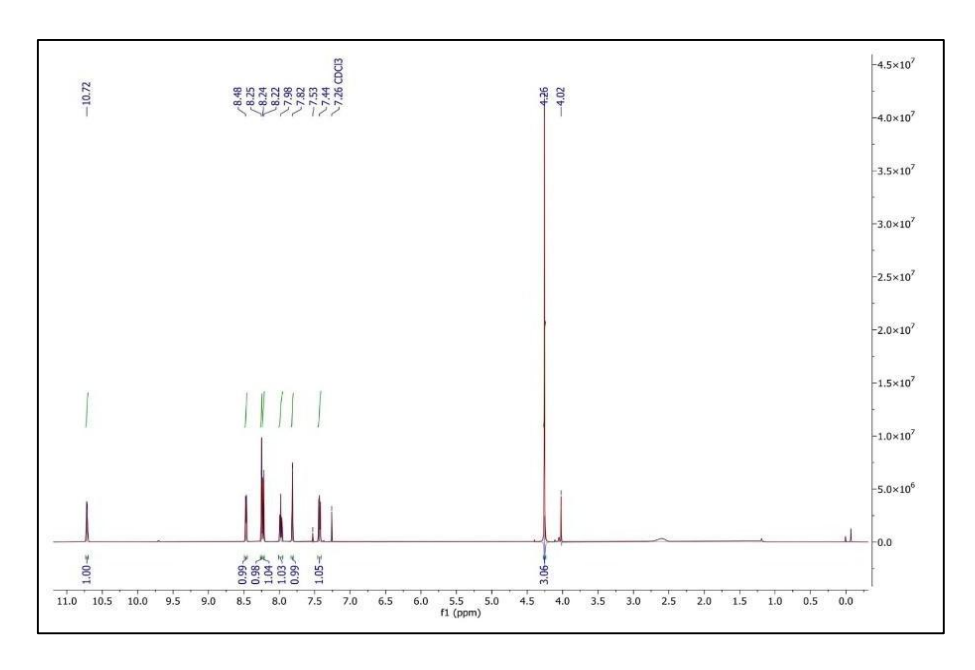


Fig. 14: ¹H NMR of Precursor P2

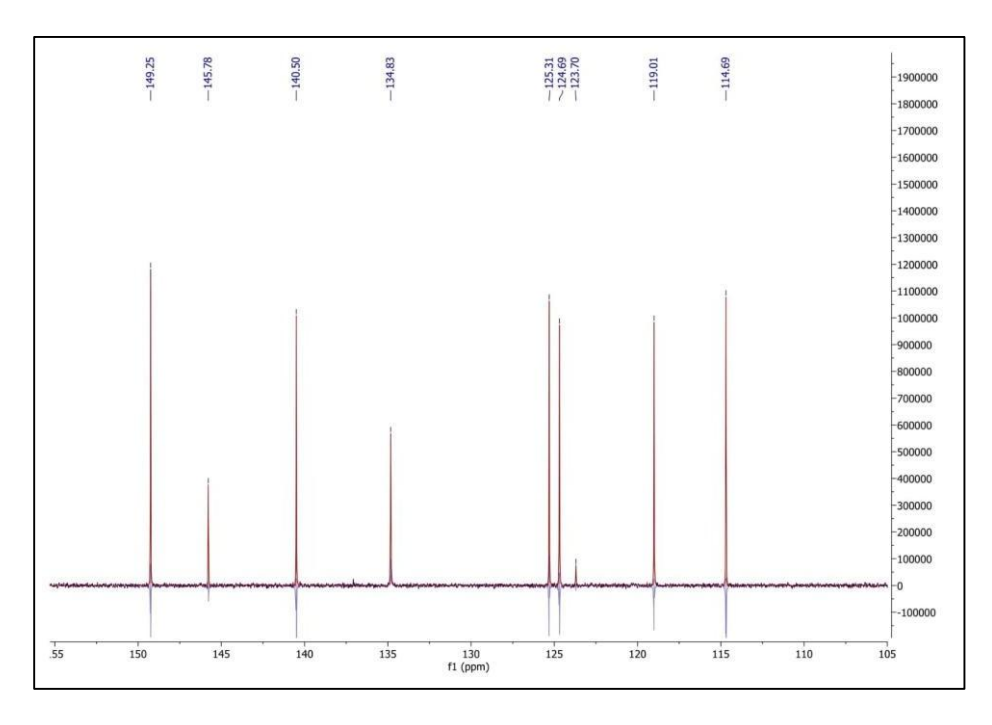


Fig. 15: ¹³C { ¹H } NMR of Precursor **P2**

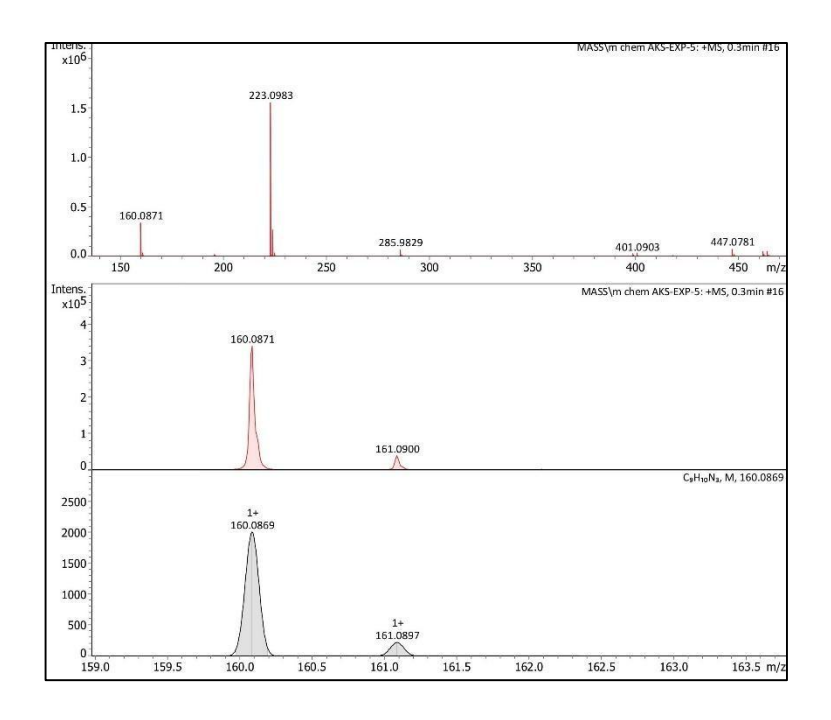


Fig. 16. LC-MS of Precursor P2

3.10 Characterization of Precursor P3

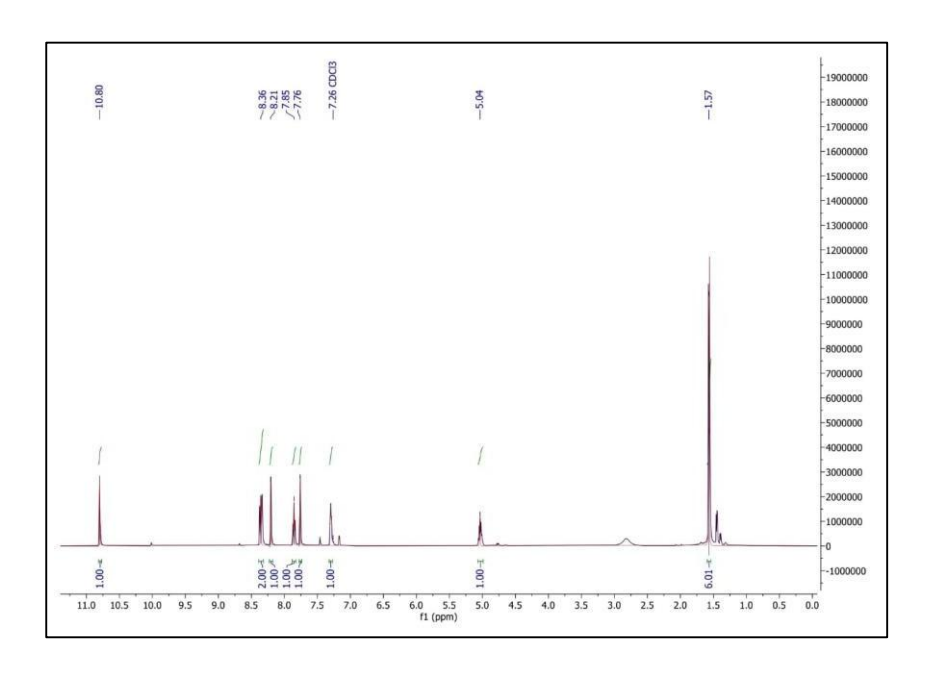


Fig. 17: ¹H NMR of Precursor P3 in CDCl₃

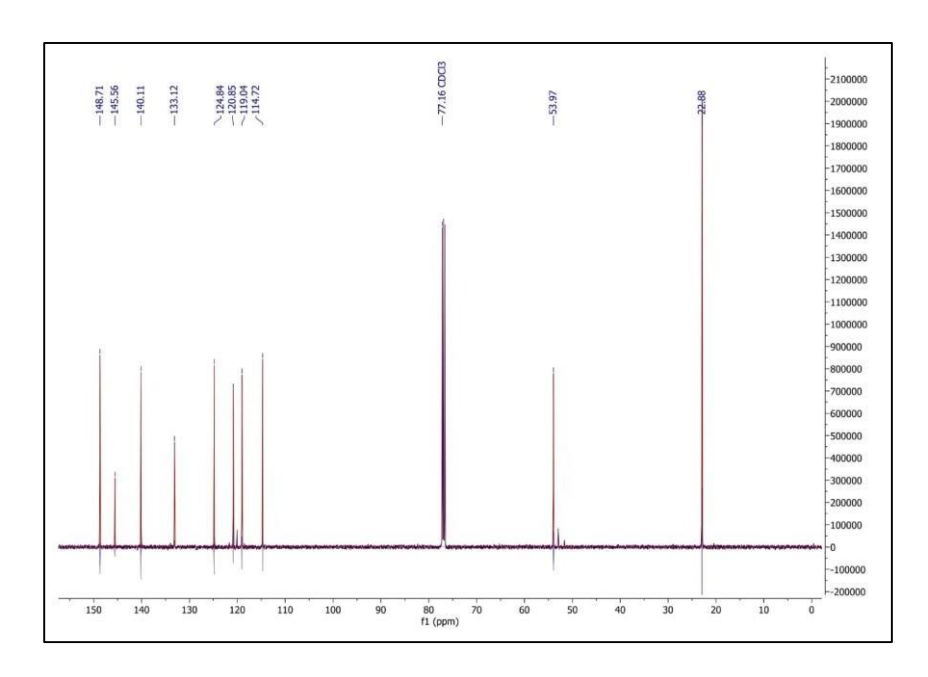


Fig. 18: ¹³C {¹H} NMR of Precursor P3 in CDCl₃

3.11 Characterization of Precursor P4

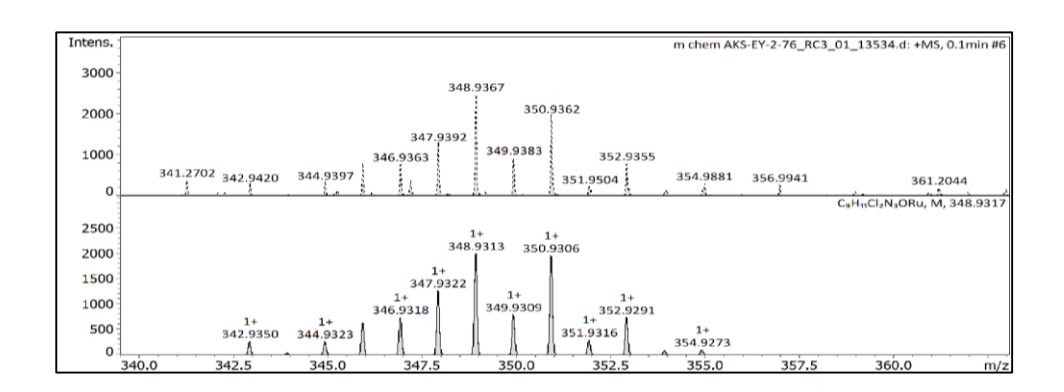


Fig. 19: LC-MS of Precursor P4

3.12 Characterization of Precursor P5

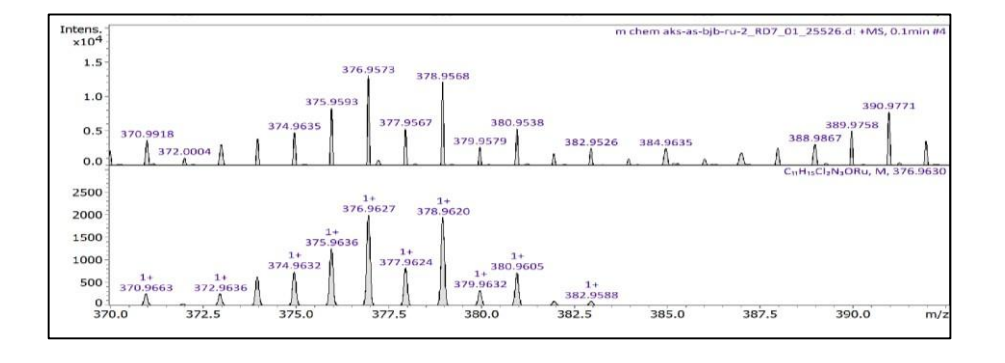


Fig. 20: LC-MS of Precursor P5

3.13 Characterization of Precursor P6

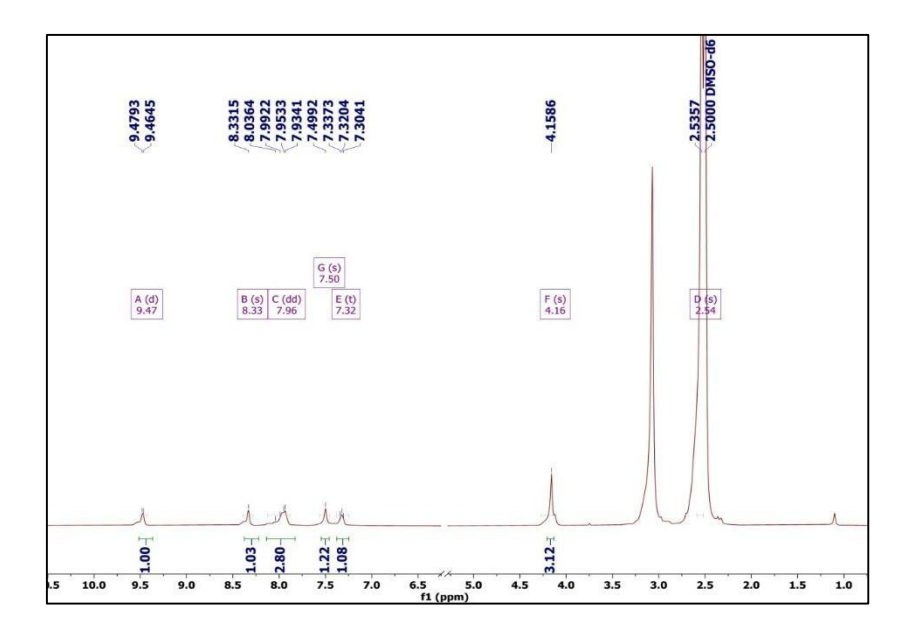


Fig. 21: ¹H NMR of Precursor P6

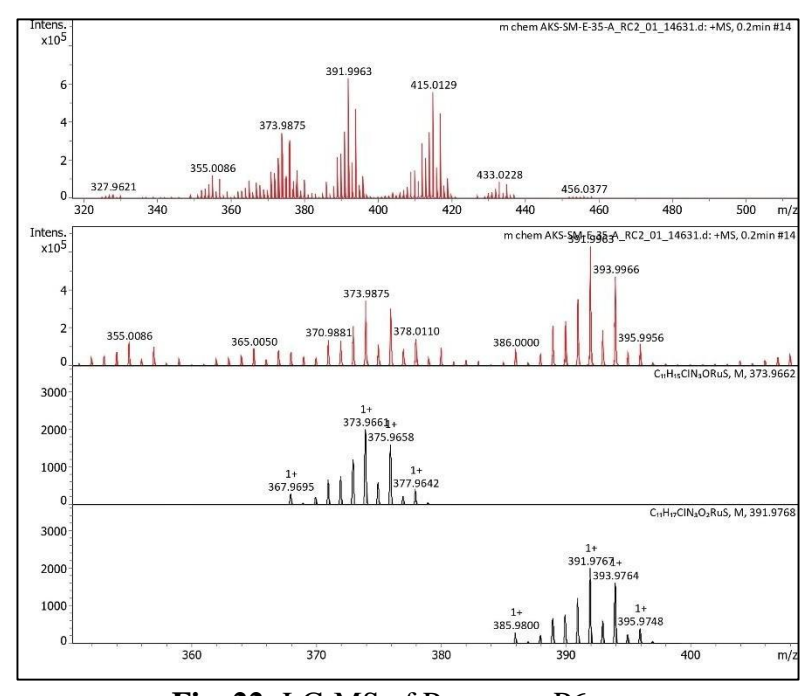


Fig. 22: LC-MS of Precursor P6

3.14 Characterization of Precursor P7

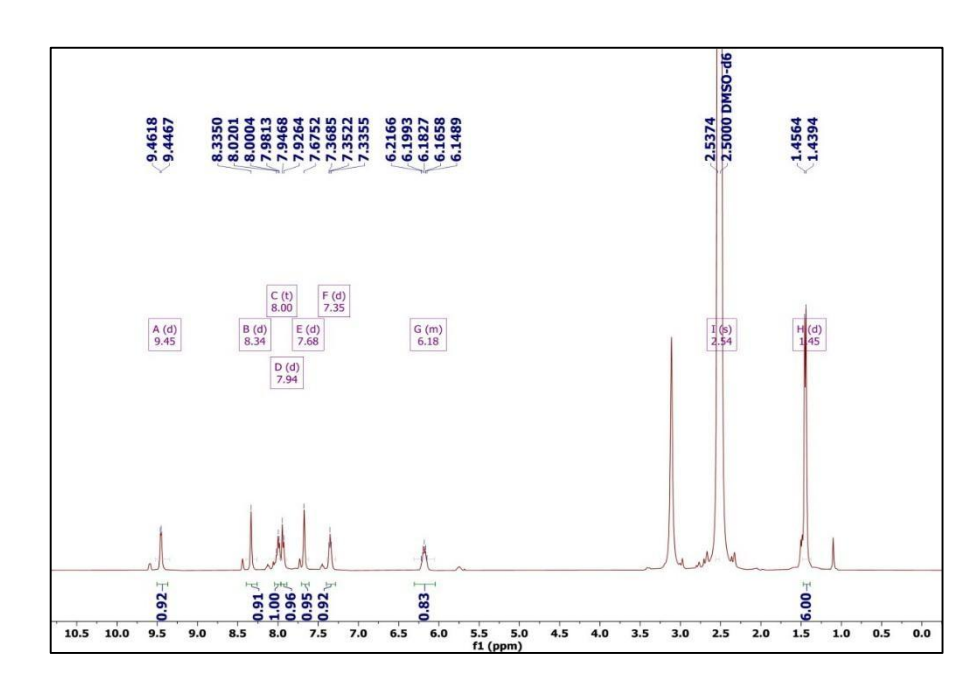


Fig. 23: ¹H NMR of Precursor P7

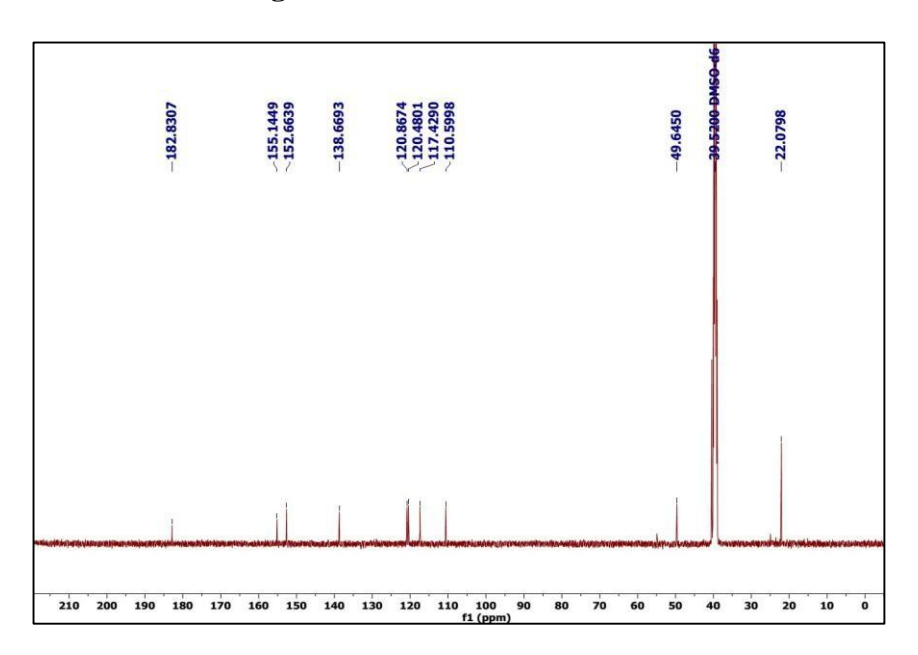


Fig. 24: ¹³C{¹H} NMR of Precursor P7

3.15 Characterization of complex Ru-1

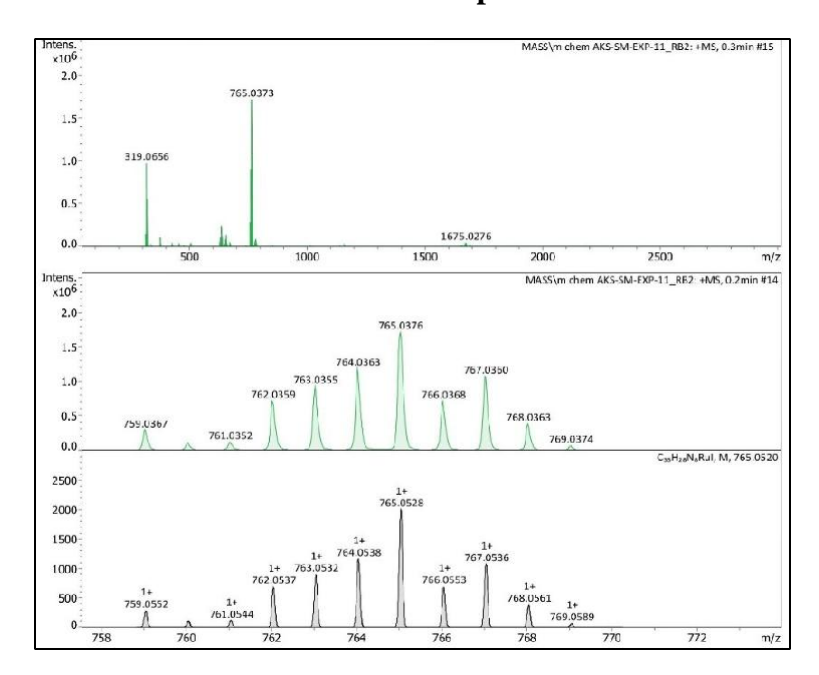


Fig. 25: LC-MS of complex Ru-1

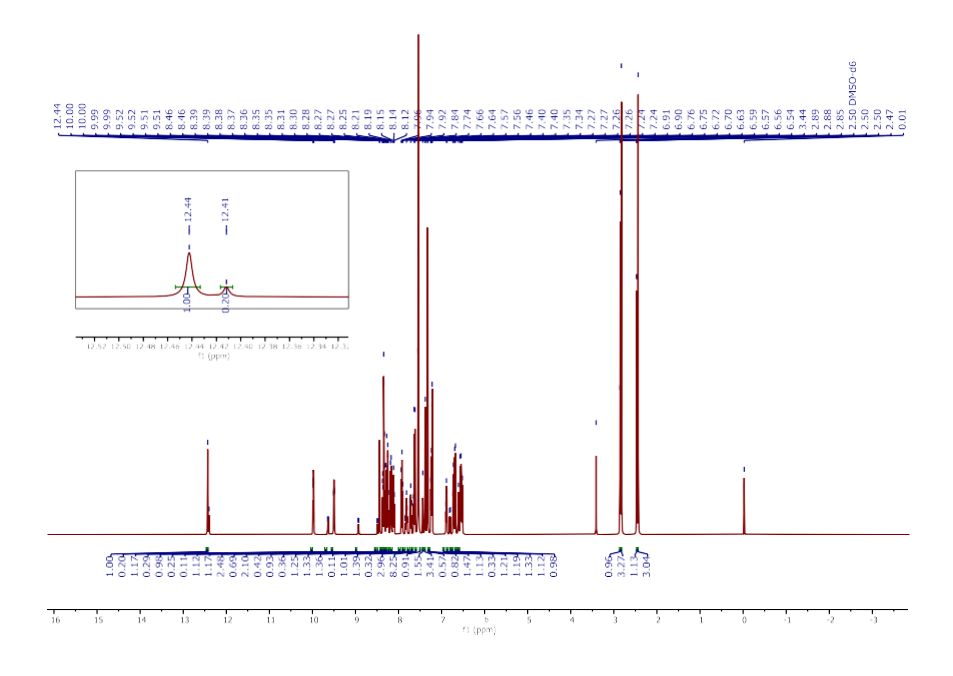


Fig. 26: ¹H NMR of complex Ru-1

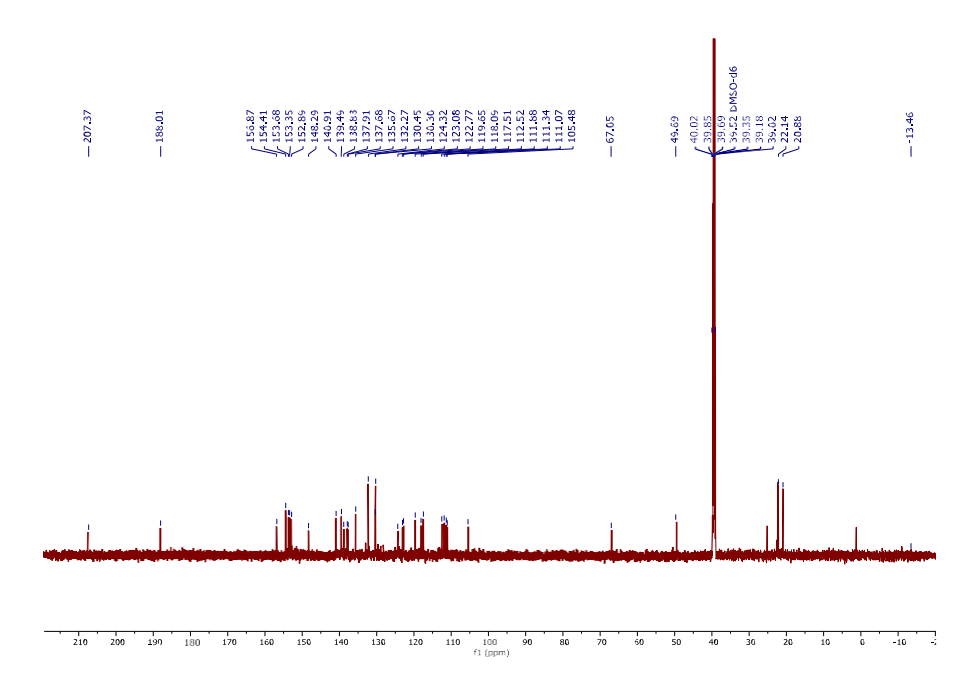


Fig. 27: 13 C $\{^{1}$ H $\}$ NMR of Complex Ru-1

3.16 Characterization of complex Ru-2

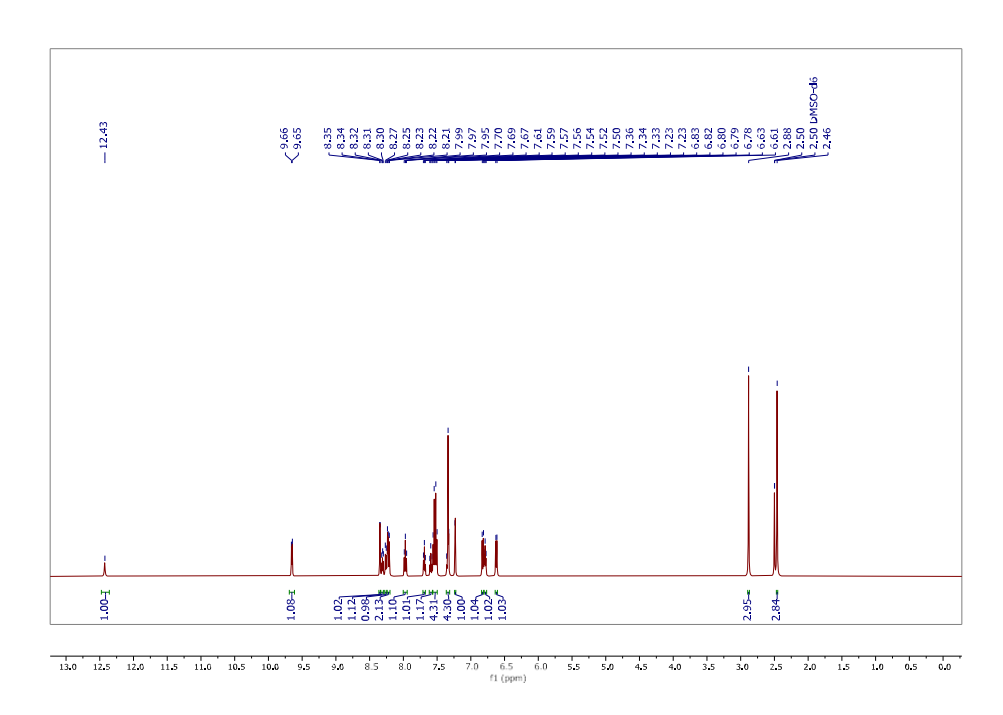


Fig. 28: ¹H NMR of complex Ru-2

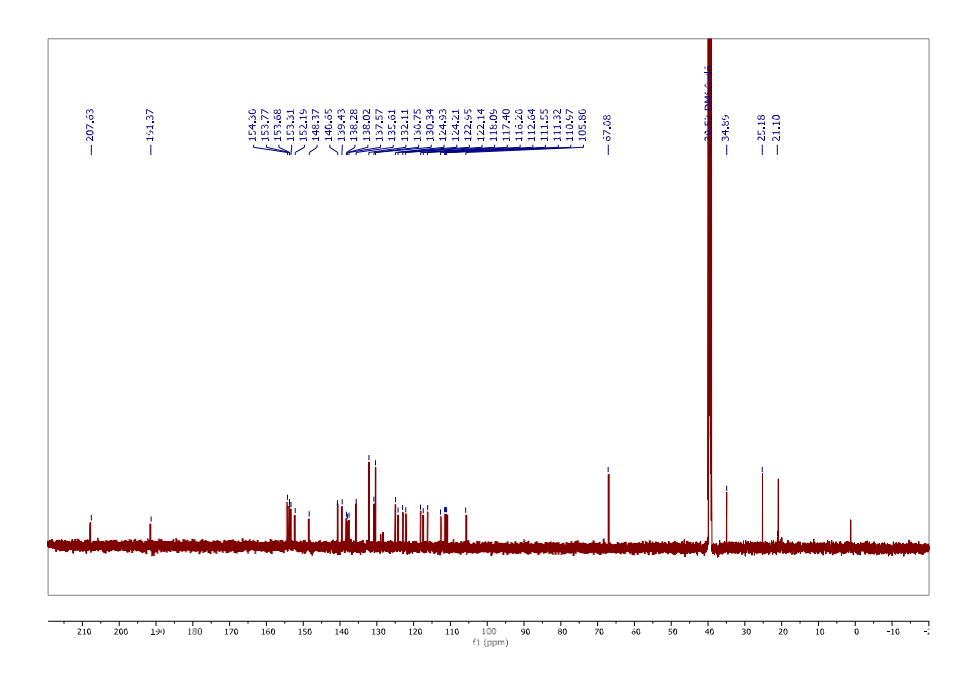


Fig. 29: ¹³C{¹H} NMR of Complex **Ru-2**

3.16.1 LC-MS of complex Ru-2

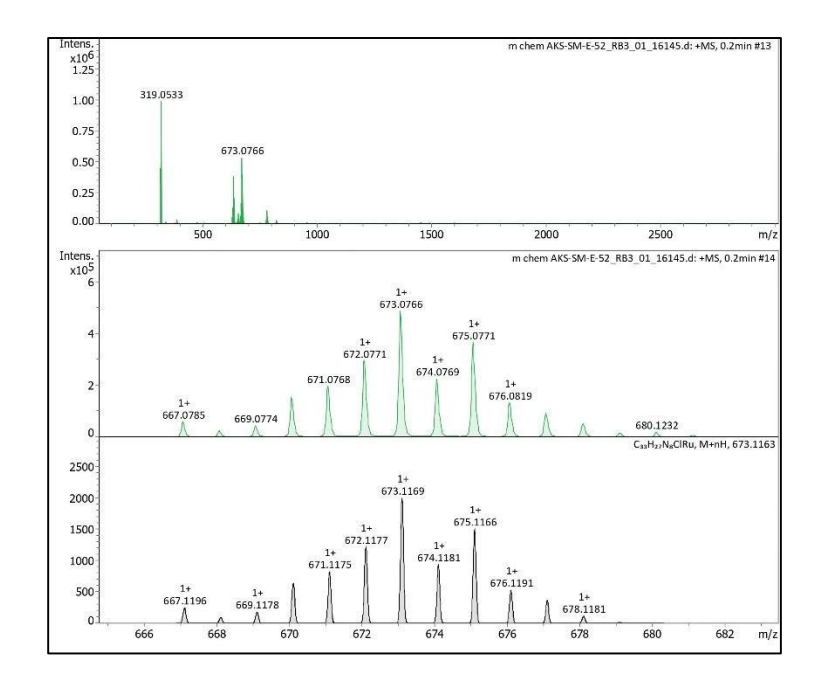


Fig. 30: LC-MS of complex Ru-2

3.17 Photoluminescent Studies

3.17.1 UV-Visible spectra of Ru-1

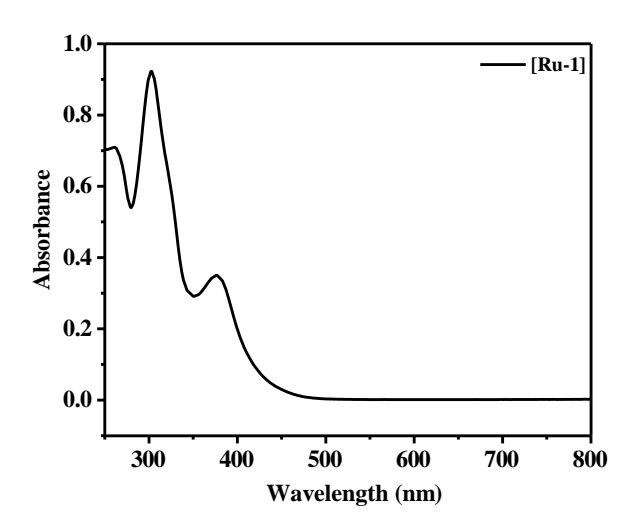


Fig. 31. UV-vis spectra of complex Ru-1 recorded in CH₃OH at room temperature.

In the UV-Vis spectra of Ru-1, 3 major peaks were observed.

- I.239: The starting peak, which corresponds to a $\pi \rightarrow \pi^*$ transition, is characteristic of the conjugated system present within the aromatic framework of the molecule.
- II.303: The most intense absorption peak observed at 303 nm in the UV-Visible spectrum is primarily attributed to a ligand-centered $\pi \rightarrow \pi^*$ transition within the conjugated pincer-NHC framework, with a possible minor contribution from a metal-to-ligand charge transfer (MLCT) involving the Ru (II) center.
- III.**376:** The weak absorption band observed at 376 nm is attributed to a metal-to-ligand charge transfer (MLCT) transition, arising from excitation of an electron from the Ru (II) d-orbitals to the π^* orbitals of the conjugated pincer-NHC ligand framework.

3.17.2 UV-Visible spectra of Ru-2

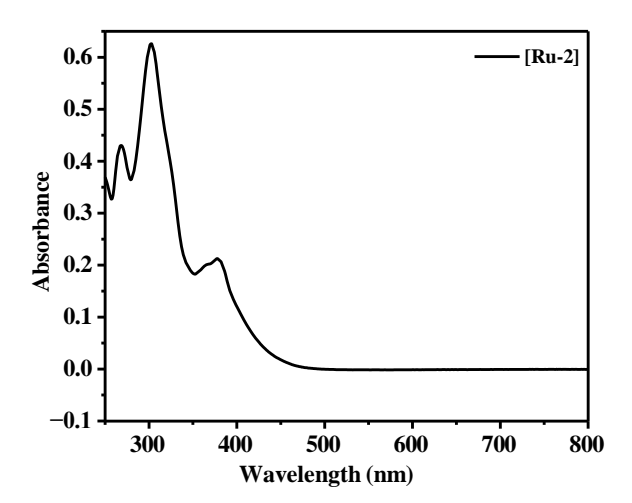


Fig. 32. UV-vis spectra of complex Ru-1 recorded in CH₃OH at room temperature.

In the UV-Vis spectra of Ru-2, 3 major peaks were observed.

- I. **271:** The intense absorption peak observed at 271 nm in the UV-Visible spectrum of the Ru-2 complex is attributed to a ligand-centered $\pi \rightarrow \pi^*$ transition, with its position reflecting the influence of the more electron-withdrawing Cl⁻ ligand, which stabilizes the π^* orbital and lowers the energy of the transition relative to the iodo analogue.
- II. **305:** The most intense absorption peak observed at 305 nm in the UV-Vis spectrum of the Ru-2 complex is assigned to a ligand-centered $\pi \rightarrow \pi^*$ transition, arising from electronic excitation within the conjugated aromatic framework of the pincer–NHC ligand.
- III. **378:** The broad and weak absorption band at 378 nm in the Ru-2 complex is assigned to a metal-to-ligand charge transfer (MLCT) transition from Ru (II) d-orbitals to π^* orbitals of the pincer–NHC ligand, with the bathochromic shift relative to the iodo analogue reflecting the influence of the more electron-withdrawing chlorido ligand.

3.17.3 Emission Spectra

Both complexes were found to be light yellow emissive under UV light in the solid state. To investigate the photoluminescent properties, solid-state emission spectra were recorded at room temperature. Broad emission and excitation spectra were observed for both Ru-1 and Ru-2. This Emission spectrum is recorded in CH₃CN.

 $Ru(NNC)(NC^{Me})I]PF_6(\mathbf{Ru-1})$

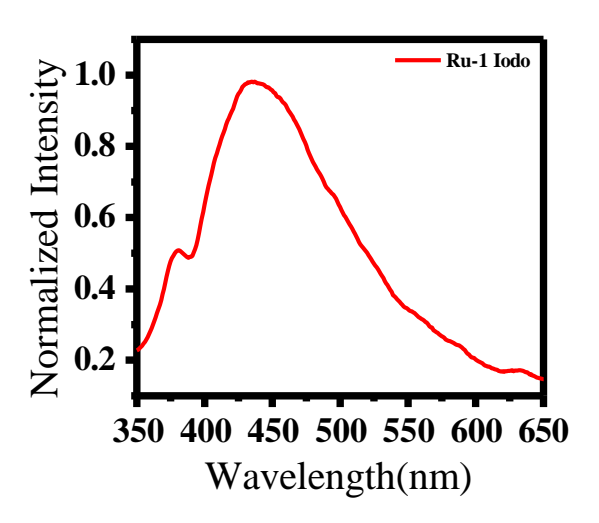


Fig. 33. Emission spectra of complex Ru-1 recorded in CH₃CN at room temperature.

The emission spectrum of Ru-1 exhibited two distinct peaks at 380 nm and 435 nm, with the latter representing the λ_{max} . The shift from 380 nm to 435 nm indicates a red shift, suggesting a change in the electronic environment of the complex, possibly due to ligand substitution or structural reorganization around the metal center.

In the emission spectrum, a minor peak was observed at 380 nm, suggesting that in the Ru-1 complex, the iodo ligand at the sixth coordination site has been substituted by DMSO. Since the iodo ligand is relatively labile and can dissociate easily, this substitution is plausible. However, the low concentration of the species accounts for the weak intensity observed in the emission spectrum.

$Ru(NNC)(NC^{Me})Cl]PF_6(\mathbf{Ru-2})$

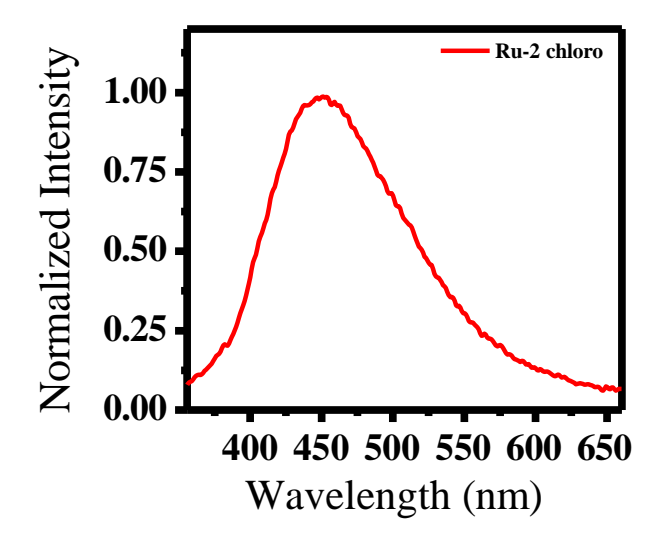


Fig. 34. Emission spectra of complex Ru-2 recorded in CH₃CN at room temperature.

The emission spectrum displays a broad fluorescence peak centered at 450 nm, which corresponds to the λ_{max} of the complex. This broad and red-shifted emission is indicative of strong π -back-donation from the Ru(II) center to the coordinated ligands, suggesting potential applicability in photophysical or photocatalytic processes.

3.18 Electrochemical Studies of Ruthenium Complexes

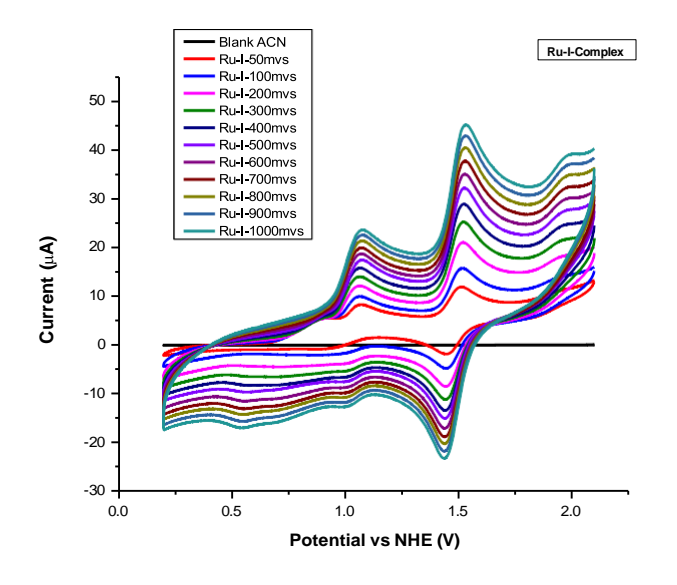


Fig. 35. Cyclic voltammograms of Ru-1 in 0.1 M TBAPF₆ recorded in CH₃CN, at scan rates between 50 mV/s to 1000 mV/s.

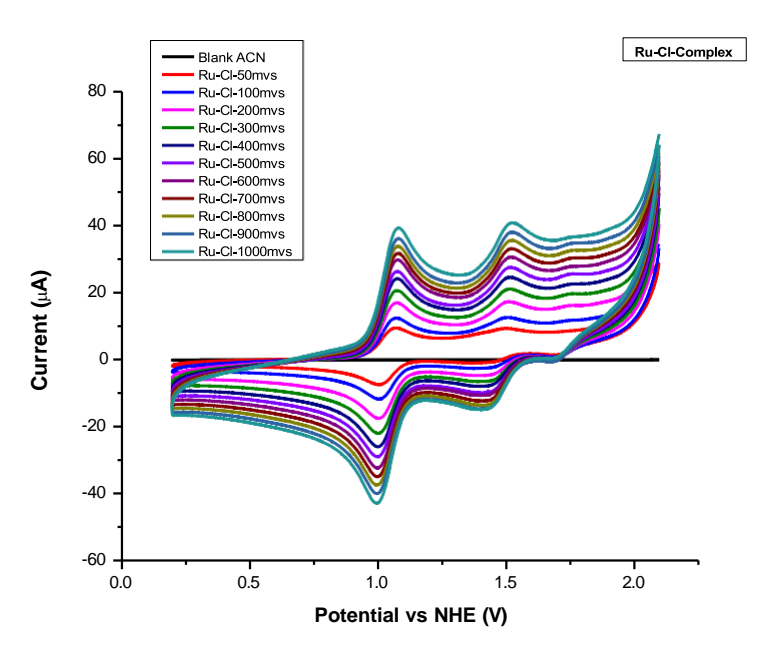


Fig. 36. Cyclic voltammograms of Ru-2 in 0.1 M TBAPF₆, recorded in CH₃CN at scan rates between 50 mV/s to 1000 mV/s.

This graph shows cyclic voltammograms of a ruthenium-chloride complex (Ru-Cl-Complex) at different scan rates. The x-axis represents potential versus NHE (Normal Hydrogen Electrode) measured in volts (V), ranging from approximately 0.0 to 2.2 V. The y-axis shows current in microamperes (μA), ranging from about -60 to +80 μA. Multiple overlaid curves represent the same Ru-Cl complex measured at different scan rates, ranging from 50 mV/s to 1000 mV/s, as indicated in the legend. The black line at the bottom represents a blank acetonitrile (ACN) control measurement. In case of Ru-1, a small redox process around 0.8-1.0 V along with a more pronounced redox couple around 1.4-1.6 V and another redox process around 1.8-2.0 V. Two distinct redox couples (peaks) are visible, the first redox couple appears around 1.7-1.9 V in Ru2.

As the scan rate increases (from 50 to 1000 mV/s), the peak currents increase proportionally, and the peaks shift slightly. This behaviour is typical in cyclic voltammetry and indicates diffusion-controlled electrochemical processes. The increase in peak current with scan rate follows the Randles-Sevcik equation, which relates peak current to the square root of the scan rate.

This electrochemical data likely represents the oxidation/reduction behaviour of the ruthenium complex, showing multiple accessible redox states typical for transition metal complexes.

3.19 CATALYTIC APPLICATIONS:

3.19.1 Amine double-dehydrogenation via [Ru-2] catalyst

Reaction Scheme:

Scheme 11: Conversion of Benzylamine to Benzonitrile

Experimental procedure: A ruthenium catalyst [Ru-2] (0.01 mmol, 8.18 mg) was added to a Schlenk tube, followed by KO^tBu (1 mmol, 112.21 mg) as the base and distilled toluene (2 mL). The setup was maintained under a nitrogen flow within a fume hood. The mixture was stirred for 5–10 minutes until a homogeneous solution was achieved. Subsequently, benzylamine (1 mmol, $109.22 \mu L$) was introduced as the substrate. The reaction mixture was then placed in a preheated silicon

Observation: The obtained product conversion was 54 %, characterized by GC-MS.

oil bath at 80 °C and allowed to react for 24 hours.

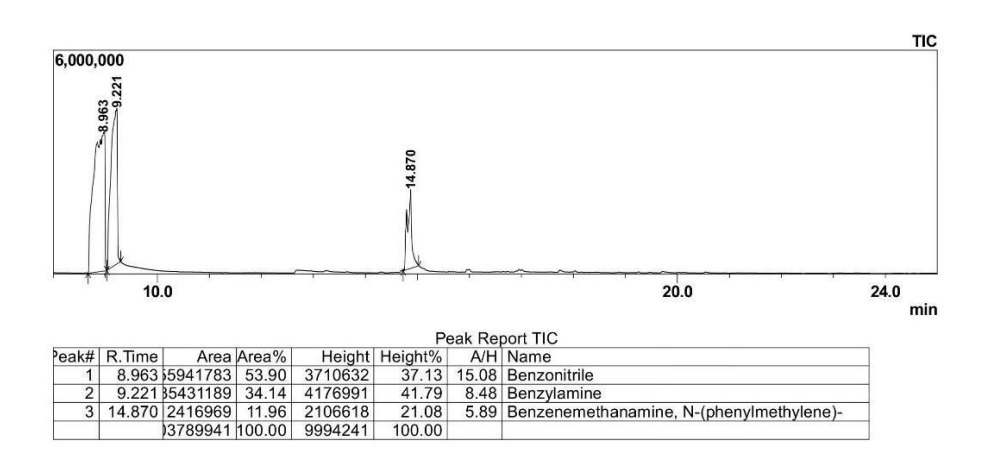
Table 1. Screening of catalyst Optimization in toluene for benzylamine double-dehydrogenation.

Entry	Catalyst	Base	Temp. (°	Conversion
	(mol%)		C)	(%)
1.	Ru-2 (1)	KO ^t Bu (1 equiv.)	80	54
2.	Ru-2 (1)	KO ^t Bu (1 equiv.)	90	67
3.	Ru-2 (1)	KO ^t Bu (1 equiv.)	90	46
4.	Ru-2 (1)	KO ^t Bu (1 equiv.)	90	40
5.	Ru-2 (0.5)	KO ^t Bu (1 equiv.)	90	91
6.	Ru-2 (0.5)	KO ^t Bu (1 equiv.)	90	65
7.	Ru-1 (1)	KO ^t Bu (1 equiv.)	90	62

Reaction Condition: Benzylamine, Catalyst (0.5 & 1 mol%), KO^tBu, and toluene (2 mL) heated in a sealed tube at a temperature (°C) and duration is 24h.

Conversion was determined by gas chromatography (GC-MS).

GC-MS spectra for screening of catalyst optimization in toluene for double-dehydrogenation of benzonitrile for **Table 1**.



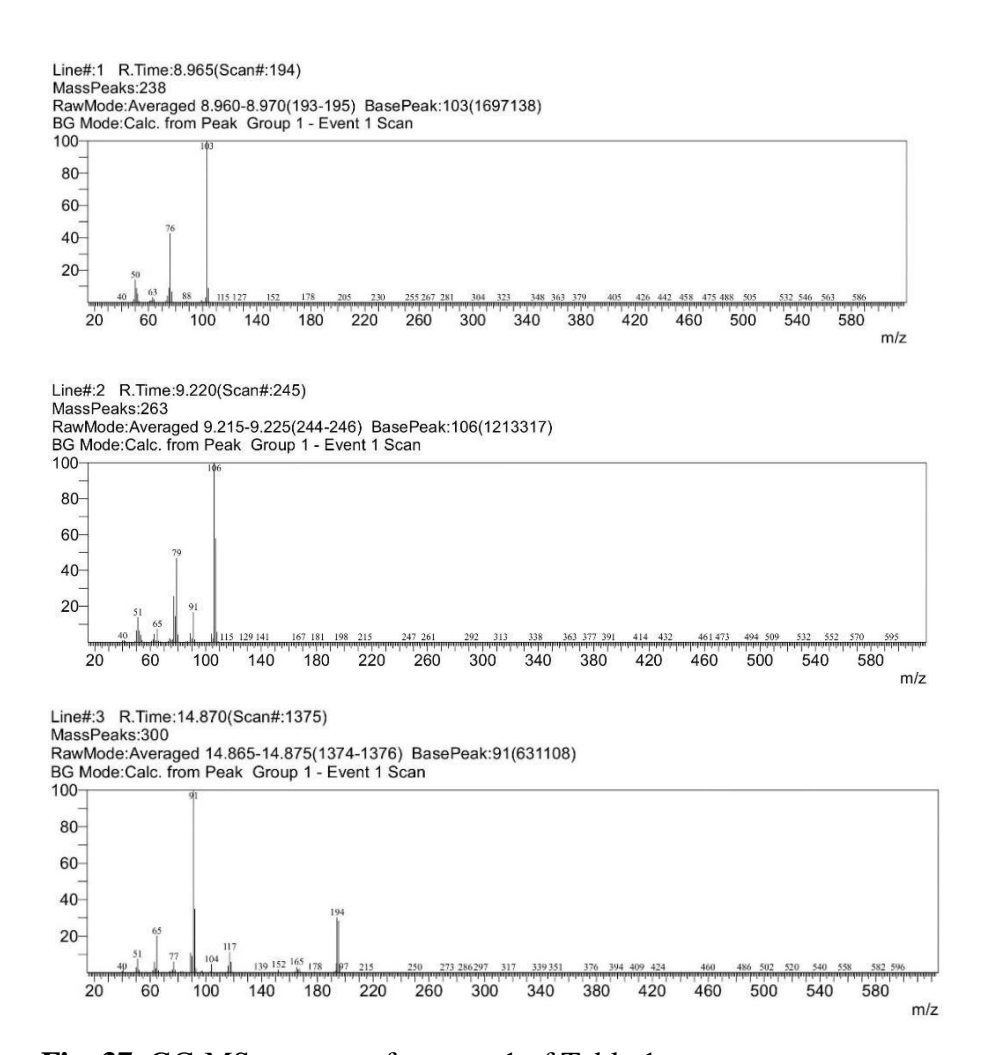
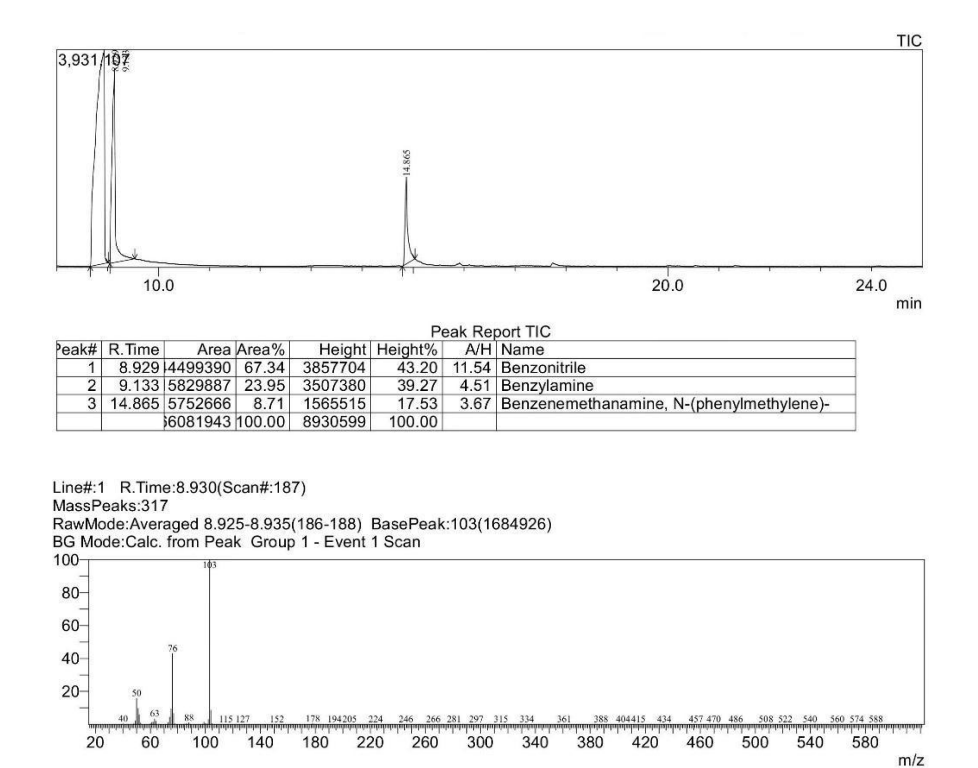


Fig. 37. GC-MS spectrum for entry 1 of Table 1



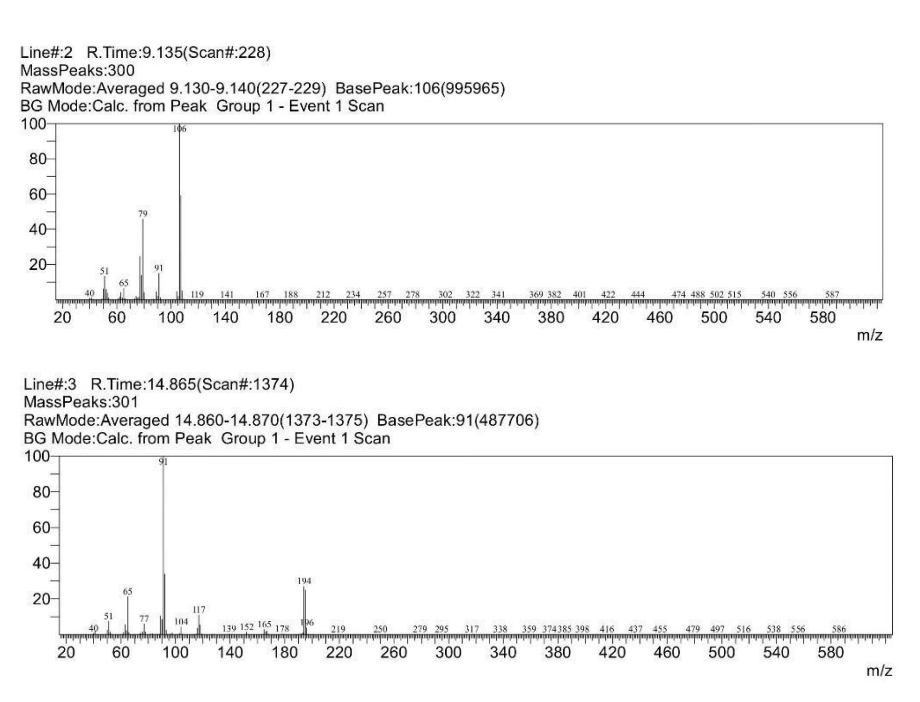
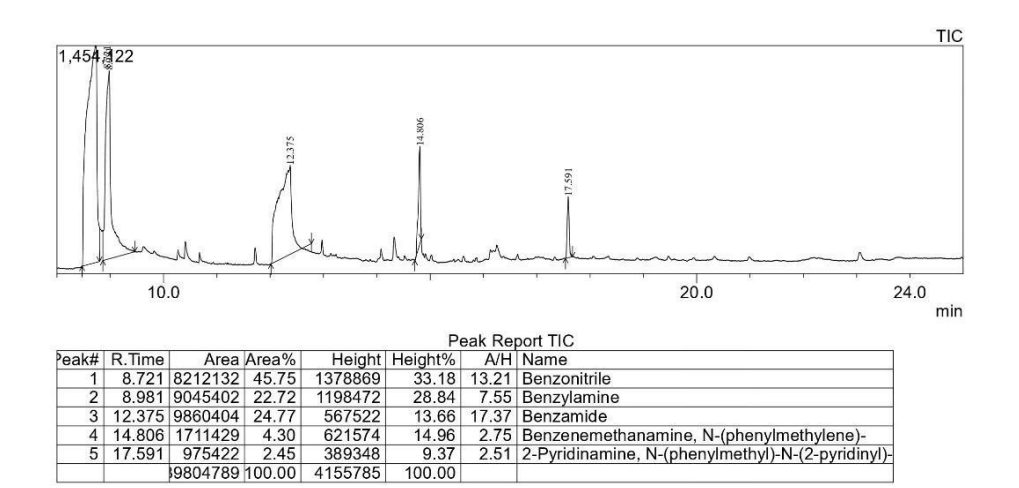
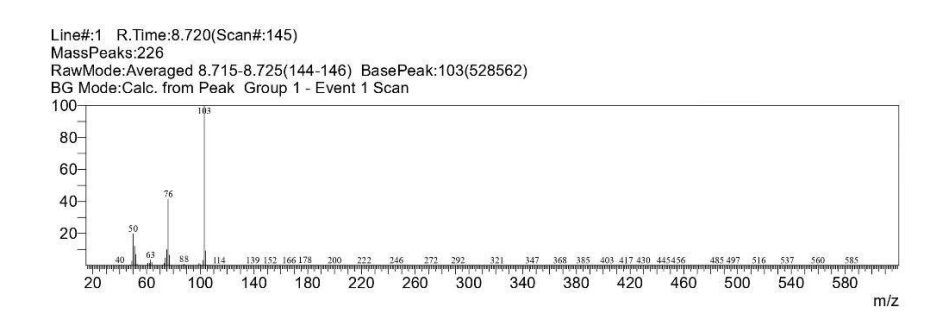


Fig. 38. GC-MS spectrum for entry 2 of Table 1





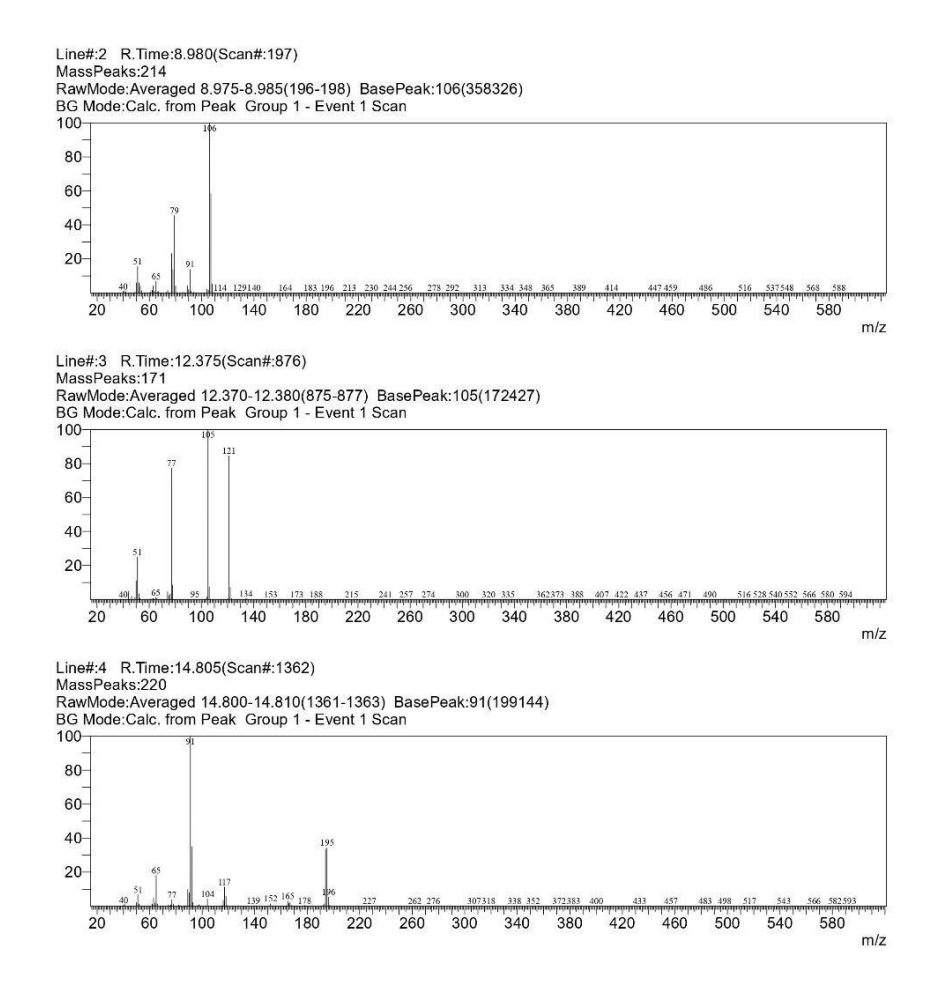
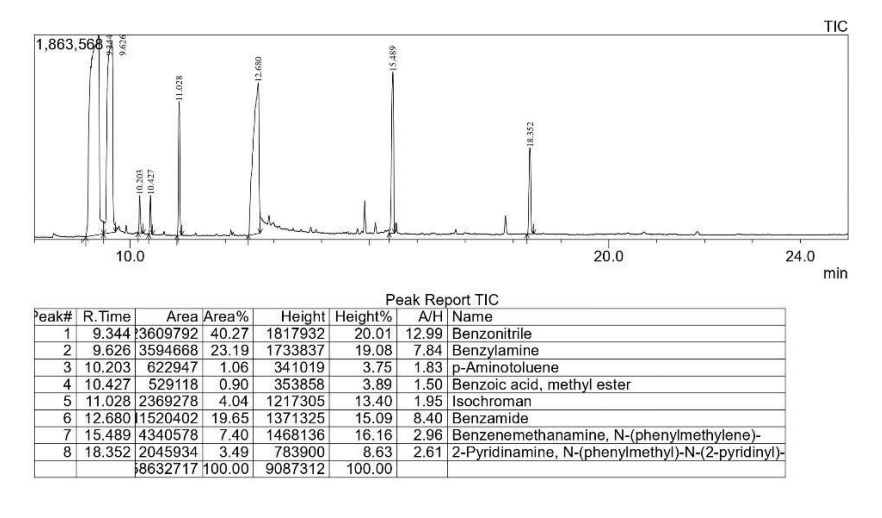
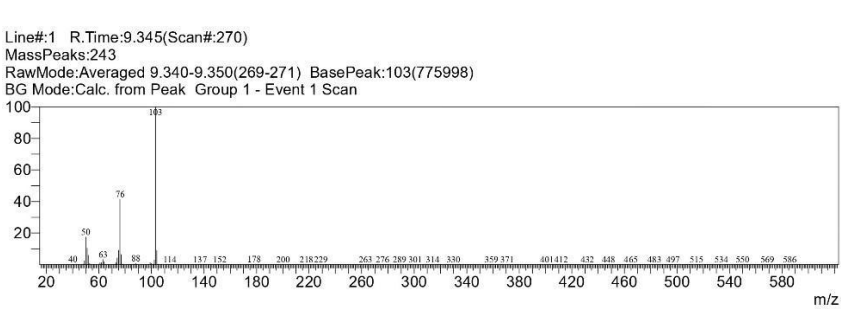


Fig. 39. GC-MS spectrum for entry 3 of Table 1





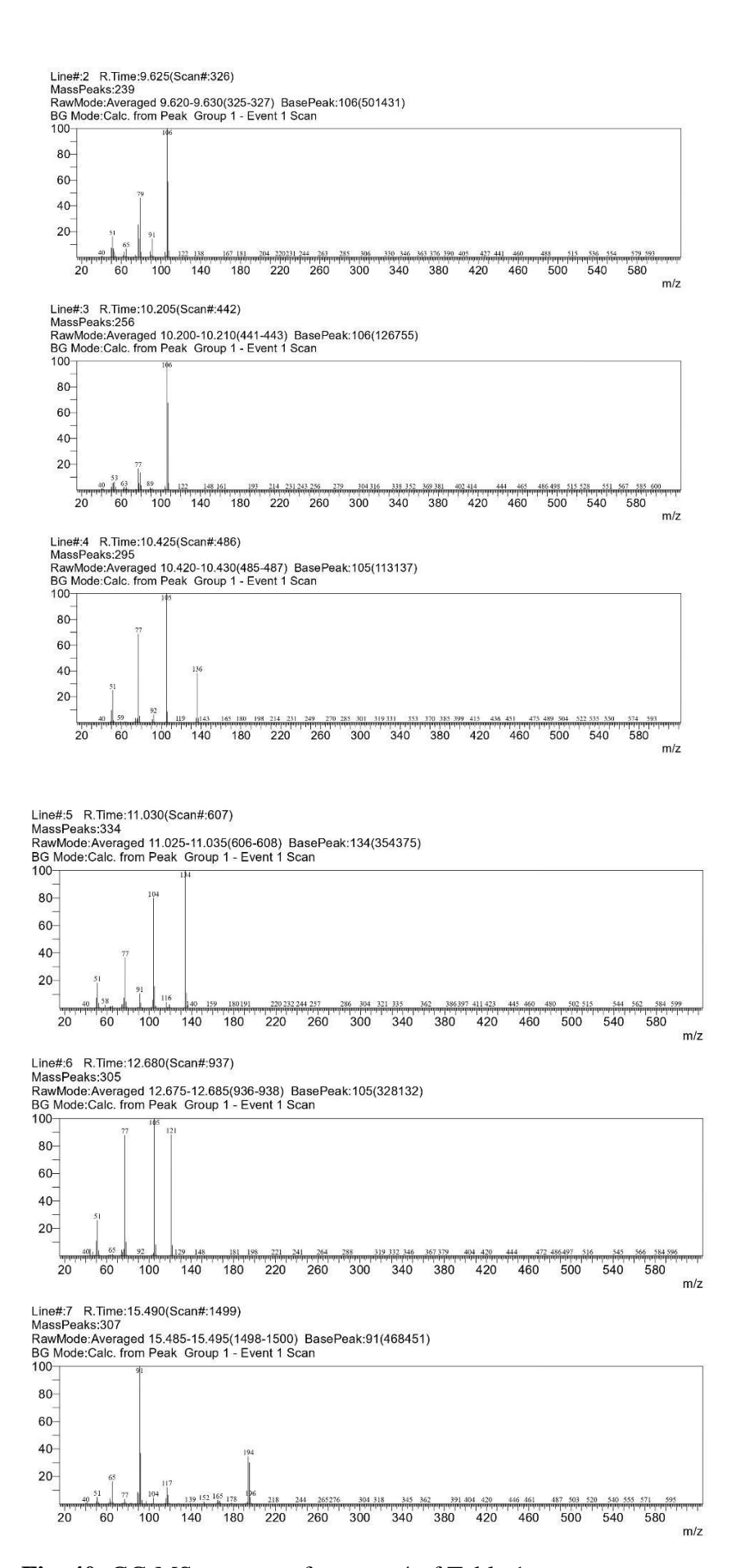


Fig. 40. GC-MS spectrum for entry 4 of Table 1

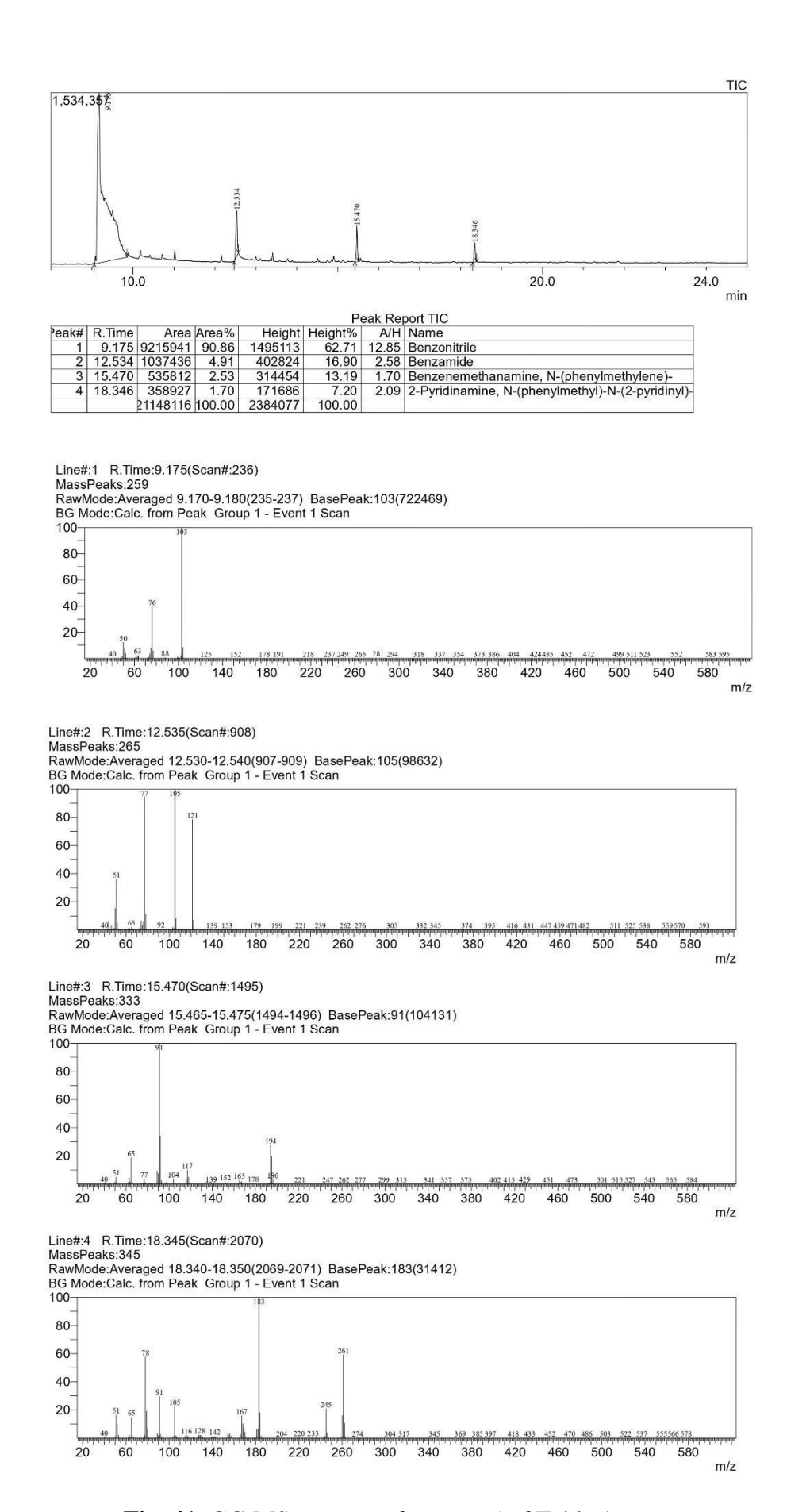


Fig. 41. GC-MS spectrum for entry 5 of Table 1

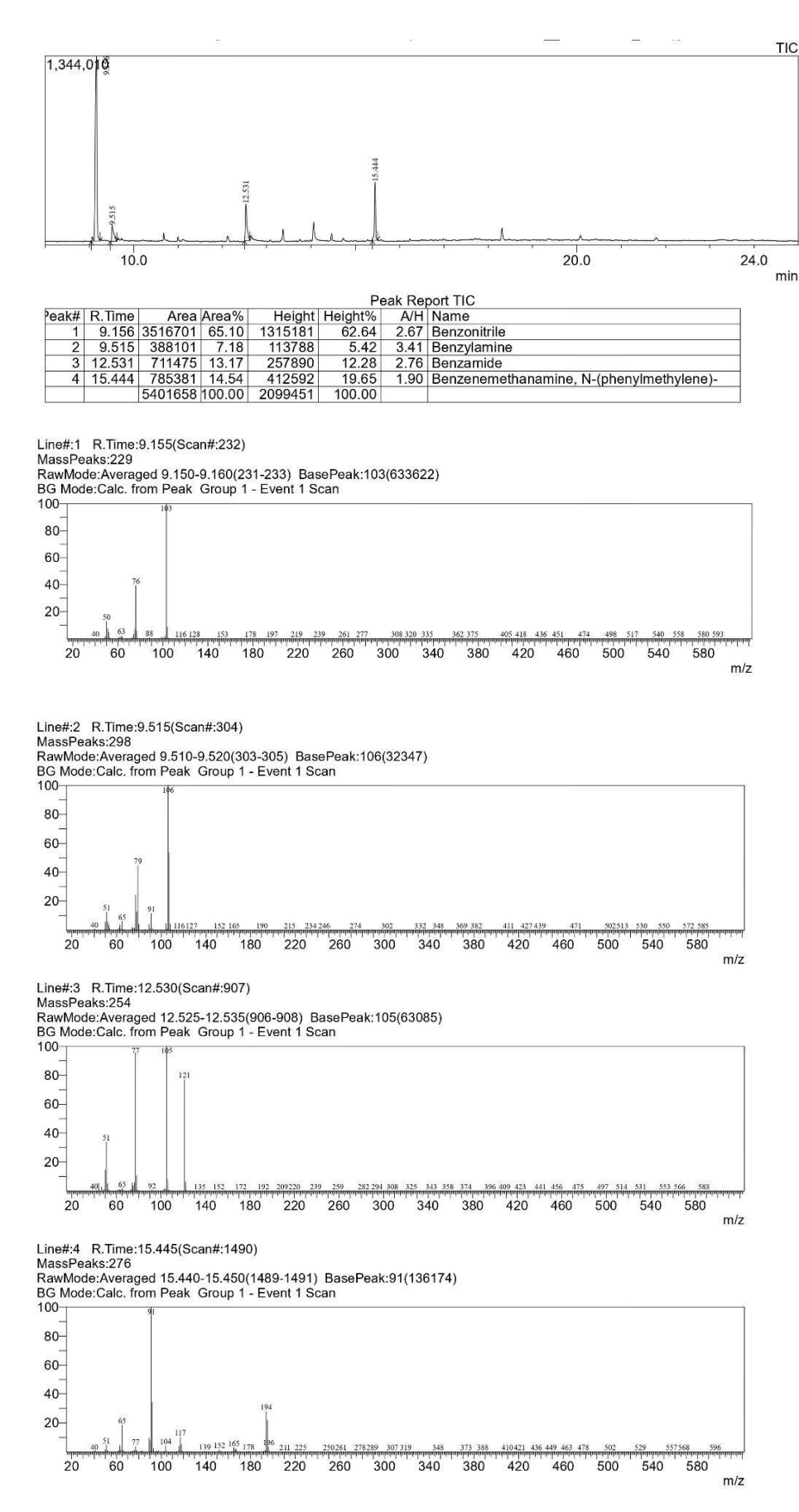
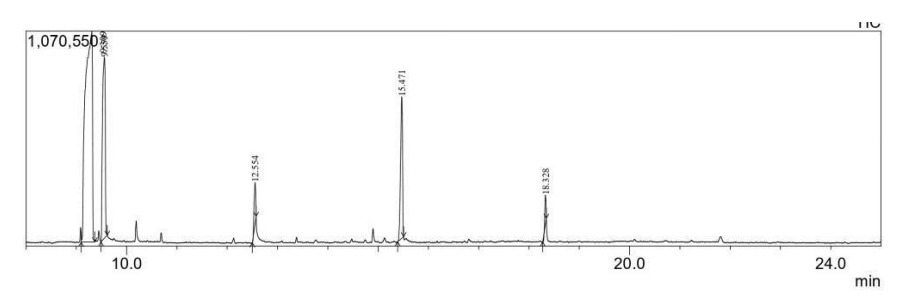


Fig. 42. GC-MS spectrum for entry 6 of Table 1



 k#
 R.Time
 Area Area
 Height

 1
 9.309
 0028842
 62.43
 1049847

 2
 9.559
 3416076
 21.27
 901946

 3
 12.554
 445595
 2.77
 204653

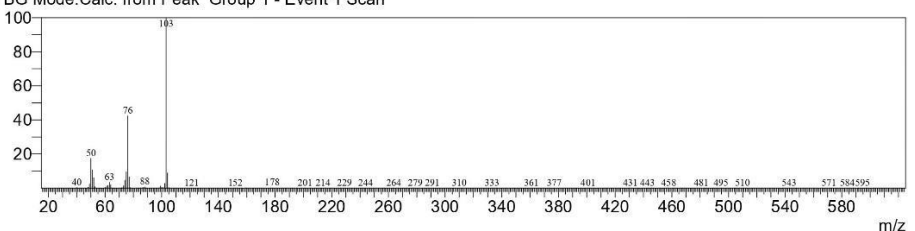
 4
 15.471
 1942230
 12.09
 705558

 5
 18.328
 230862
 1.44
 143841

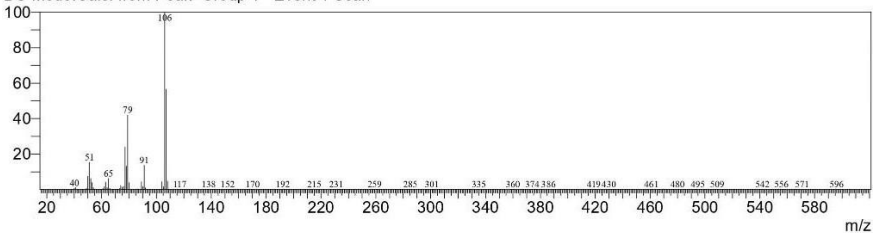
 6063605
 100.00
 3005845
 eak# R.Time

Line#:1 R.Time:9.310(Scan#:263) MassPeaks:255

MassPeaks:250 RawMode:Averaged 9.305-9.315(262-264) BasePeak:103(456668) BG Mode:Calc. from Peak Group 1 - Event 1 Scan

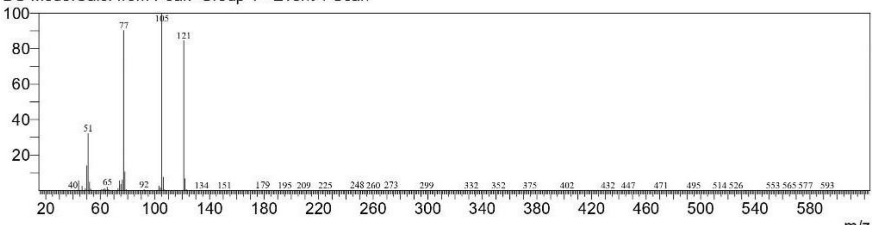


Line#:2 R.Time:9.560(Scan#:313)
MassPeaks:269
RawMode:Averaged 9.555-9.565(312-314) BasePeak:106(272794)
BG Mode:Calc. from Peak Group 1 - Event 1 Scan



Line#:3 R.Time:12.555(Scan#:912) MassPeaks:266

National RawMode: Averaged 12.550-12.560(911-913) BasePeak: 105(50259) BG Mode: Calc. from Peak Group 1 - Event 1 Scan



Line#:4 R.Time:15.470(Scan#:1495) MassPeaks:263

RawMode:Averaged 15.465-15.475(1494-1496) BasePeak:91(220664) BG Mode:Calc. from Peak Group 1 - Event 1 Scan 80-60-40-20-20 60 100 140 180 220 260 300 340 380 420 460 500 540 m/z

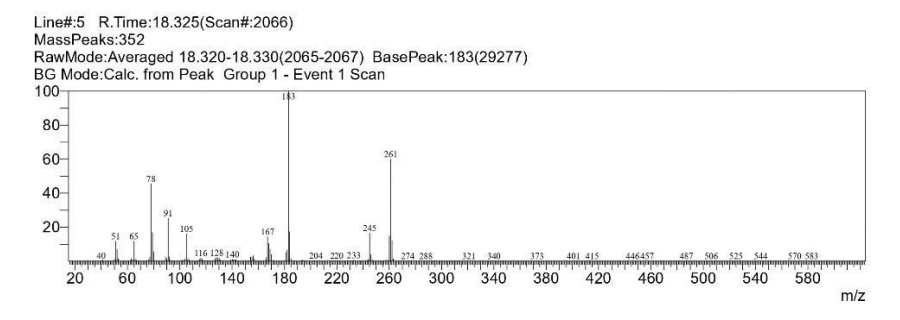


Fig. 43. GC-MS spectrum for entry 7 of Table 1

3.19.2 Hydration of Nitriles via [Ru-2] catalyst

Reaction Scheme:

Scheme 12: Conversion of Benzonitrile to Benzamide

Experimental Procedure: A dry 10 mL Schlenk tube with a magnetic bead was prepared. As the reaction is not air-sensitive, no nitrogen flow was used. [Ru-2] (0.01 mmol, 8.18 mg), NaOH (0.2 mmol, 7.98 mg), and water (5 mL) were added and stirred for 5–10 min until homogeneous. Benzonitrile (1 mmol, $103 \mu L$) was then added, and the mixture was heated at $60 \,^{\circ}$ C in an oil bath for $12–24 \, h$.

Observation: The obtained product was characterized by GC-MS.

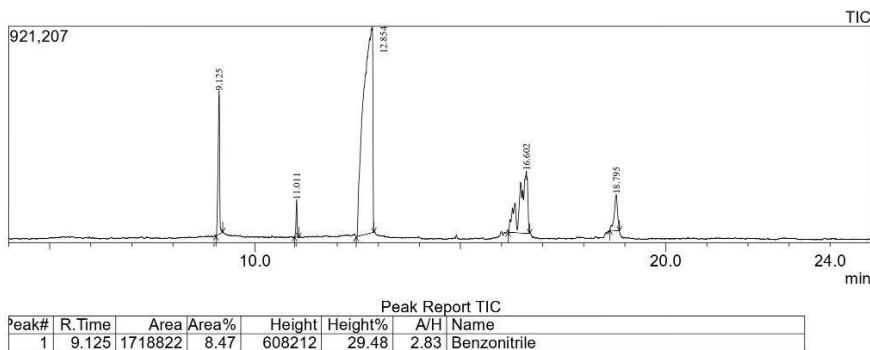
Table 2. Screening of catalyst Optimization in water for the hydration of Benzonitriles.

Entry	Catalyst (mol%)	Base (mmol)	Time (h)	Conversion (%)	
1.	Ru-2 (1)	NaOH (0.2)	24	92	
2.	Ru-2 (1)	NaOH (0.2)	12	68	
3.	Ru-2 (1)	KOH (0.2)	24	82	

Reaction Condition: Benzonitrile (1 mmol), Catalyst (1 mol%), Base, and H_2O (5 mL) under an open-air condition, heated at a temperature of 60 °C.

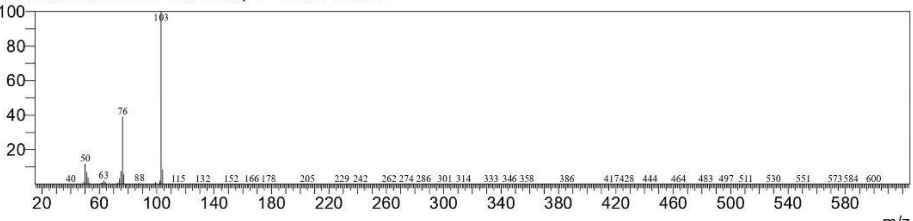
Conversion was determined by gas chromatography (GC-MS) without an internal standard.

GC-MS spectra for screening of catalyst optimization in water for hydration of benzonitrile for Table 2.



					F	ear Ive	JULI TIC	
eak#	R.Time	Area	Area%	Height	Height%	A/H	Name	
1	9.125	1718822	8.47	608212	29.48	2.83	Benzonitrile	
2	11.011	275368	1.36	158551	7.68	1.74	Isochroman	
3	12.854	3808534	68.05	876823	42.50	15.75	Benzamide	
4	16.602	3640735	17.94	265888	12.89	13.69	pyrazine, 2,3,5,6-tetraphenyl-	
5	18.795	849009	4.18	153877	7.46	5.52	RT:18.795	
		20292468	100.00	2063351	100.00			

Line#:1 R.Time:9.125(Scan#:1026) MassPeaks:241 RawMode:Averaged 9.120-9.130(1025-1027) BasePeak:103(297556) BG Mode:Calc. from Peak Group 1 - Event 1 Scan



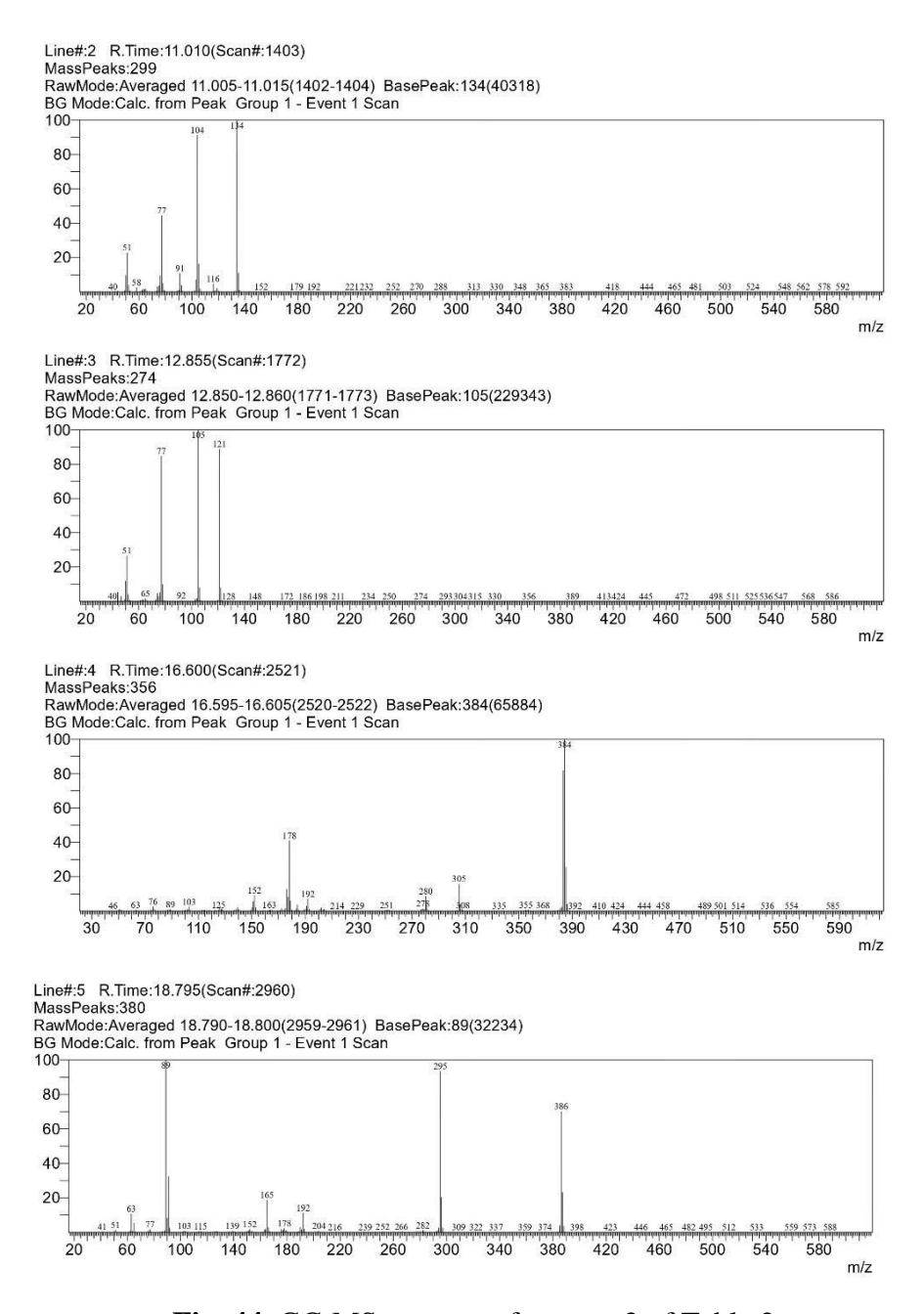
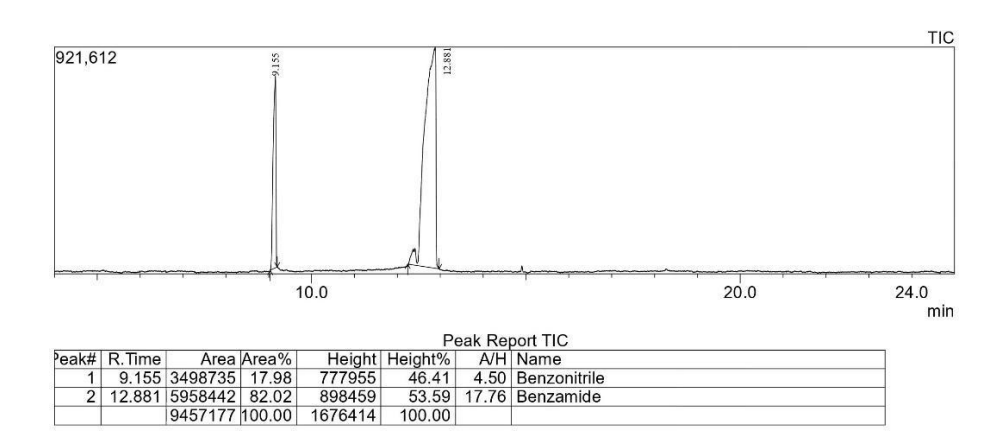


Fig. 44. GC-MS spectrum for entry 2 of Table 2



100.00

1676414

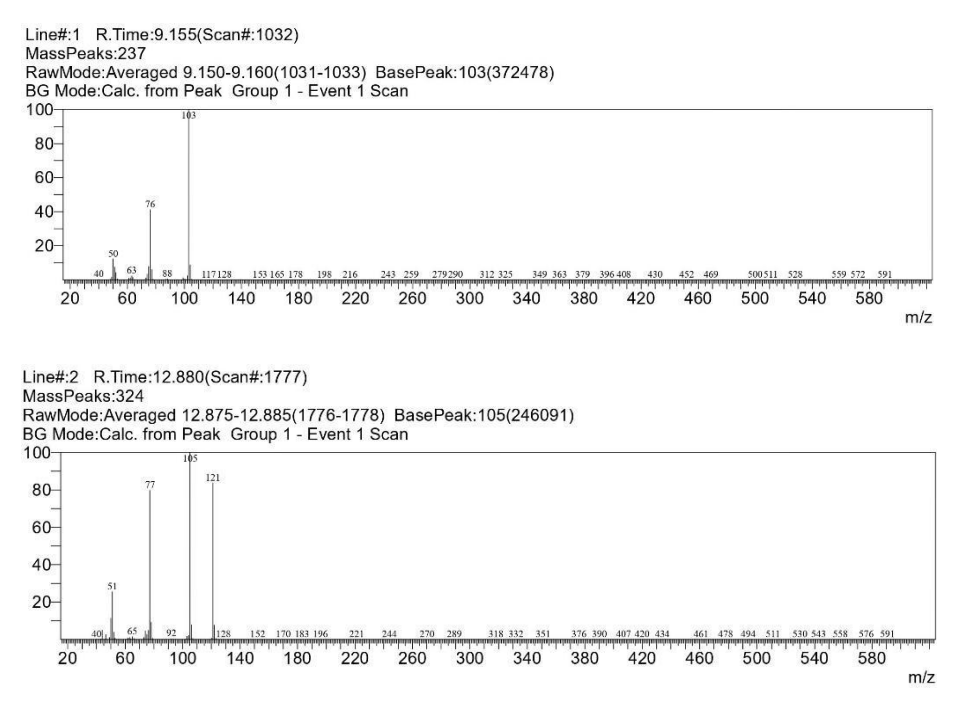


Fig. 45. GC-MS spectrum for entry 3 of Table 2

3.19.3 Water Oxidation via Ru-1 catalyst

As a part of our research, we have extensively established the process of water oxidation using the Ru-1 catalyst, including Nitric acid.

Further studies are necessary to uncover the underlying mechanisms that govern this behavior and optimize the conditions for effectively utilizing the **Ru-1** catalyst in the water oxidation reaction.

Oxygen Evolution Experiment in HNO3:

Reaction Scheme:

$$2H_2O \xrightarrow{\text{Ru-1, CAN (30 equiv.)}} O_2 + 4H + 4e^{\bigcirc}$$

Scheme 13: Oxygen evolution experiment in 0.1M HNO₃.

Experimental Procedure: To experiment, the CAN was dissolved in 0.1 M HNO₃ by stirring and purging with N₂ in a 25 mL round-

bottom flask custom-made for this purpose. The catalyst was then dissolved in ACN and added through the sidearm to complete the reaction mixture. The reaction mixture was stirred and maintained at a temperature of up to 60 °C.

Observation: During the experiment, a significant phenomenon was observed wherein the evolution of oxygen bubbles occurred over a specific temporal interval. Within the subsequent 20 minutes, a quantified volume of 4 mL of oxygen was evolved. The reaction proceeded steadily, and after 24 hours, the total volume of evolved oxygen reached 18 mL.

3.19.4 Water Oxidation as an Electrochemical Process

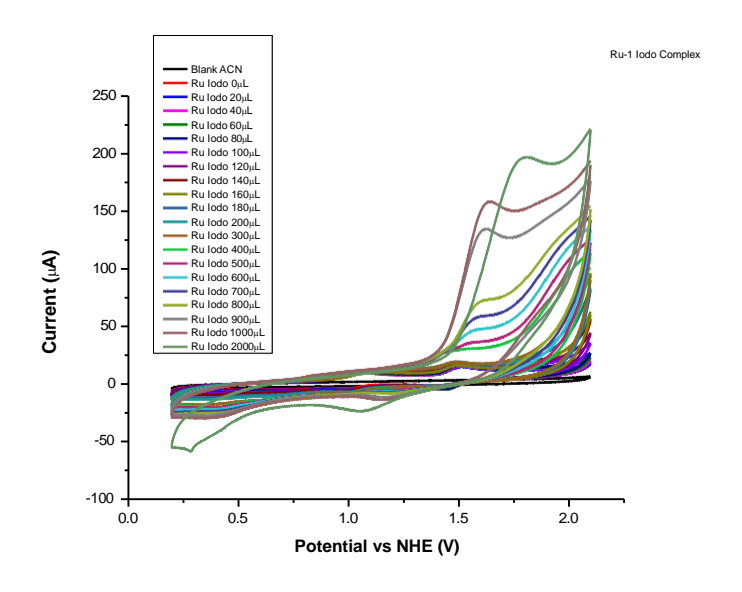


Fig. 46. Cyclic voltammograms of complex Ru-1 recorded in CH₃CN using 0.1 M TBAF₆ as the supporting electrolyte

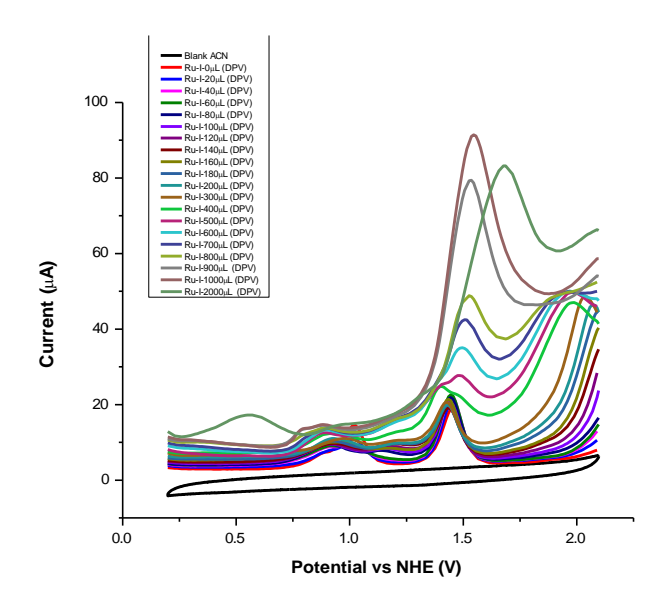


Fig. 47. DPV of complex Ru-1 recorded in CH_3CN using 0.1 M $TBAF_6$ as the supporting electrolyte

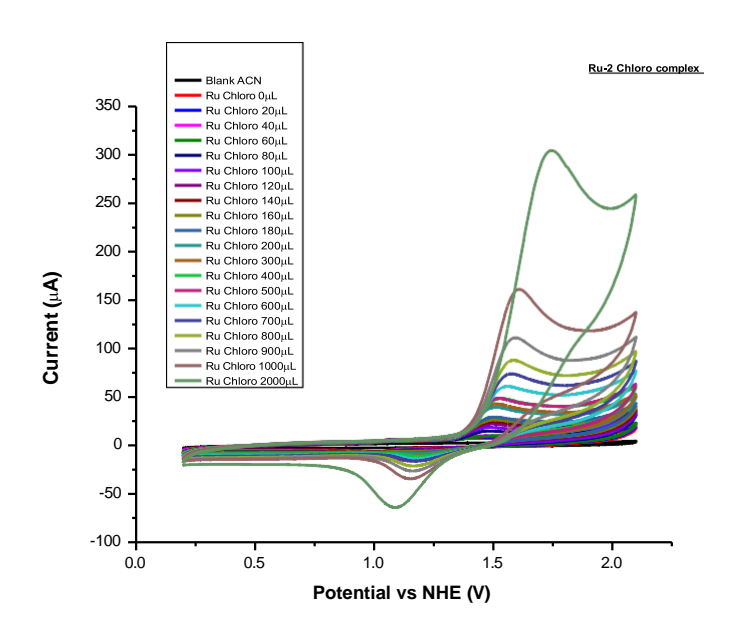


Fig. 48. Cyclic voltammograms of complex Ru-2 recorded in CH₃CN using 0.1 M TBAF₆ as the supporting electrolyte

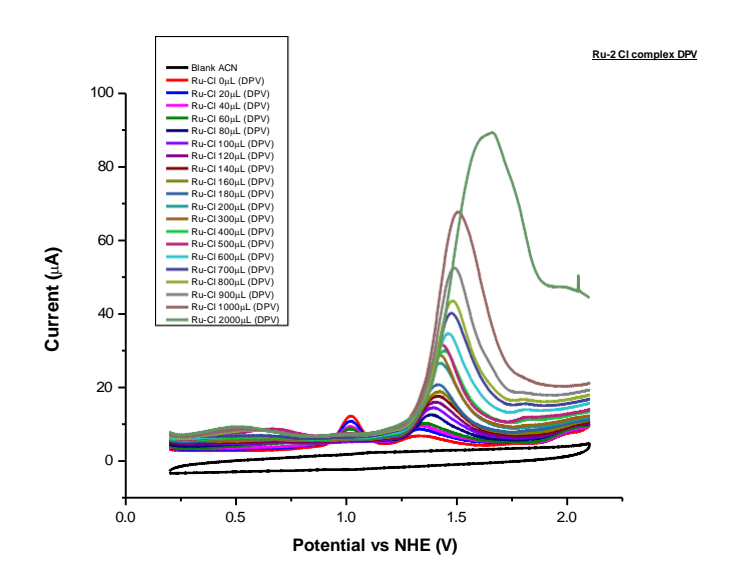


Fig. 49. DPV of complex Ru-2 recorded in CH₃CN using 0.1 M TBAF₆ as the supporting electrolyte

This graph shows cyclic voltammograms of a Ru-Chloro complex being tested for water oxidation catalysis at different scan rates. The most notable feature is the dramatic current increase beginning around 1.5V and continuing to rise steeply as the potential increases beyond 1.8V. This large anodic (positive) current wave represents water oxidation catalysis - the electrocatalytic conversion of water to oxygen $(2H_2O \rightarrow O_2 + 4H^+ + 4e^-)$. There is a small redox couple visible around 1.0-1.2V, which likely represents a Ru(II)/Ru(III) transition in the complex before the catalytic water oxidation begins. Some of the higher concentration samples show a second feature around 2.0V, which could represent additional oxidation states of the catalyst or a second catalytic process. The onset potential for water oxidation (around 1.5V vs NHE) is consistent with what's typically seen for ruthenium-based water oxidation catalysts. The large catalytic currents compared to the background processes indicate good catalytic activity of this complex toward water oxidation. These differences likely result from the electronic and structural influence of the iodide ligands versus the chloride ligands, affecting the catalytic mechanism and efficiency of the water oxidation process. The chloro complex still functions as an effective water oxidation catalyst, but with slightly different electrochemical behavior compared to its iodo counterpart.

3.19.5 Evaluation of Catalyst for Hydrogen Splitting Catalysis:

1.1 Addition of Base: KO^tBu is added as a base to a J-Young NMR tube containing the Ru-2 catalyst dissolved in DMSO-d₆, followed by mixing using a shaker.

Observation: After analyzing the ¹H NMR spectrum before and after the addition of the base, the disappearance of the protic-H peak at 12.42 ppm confirms successful deprotonation.

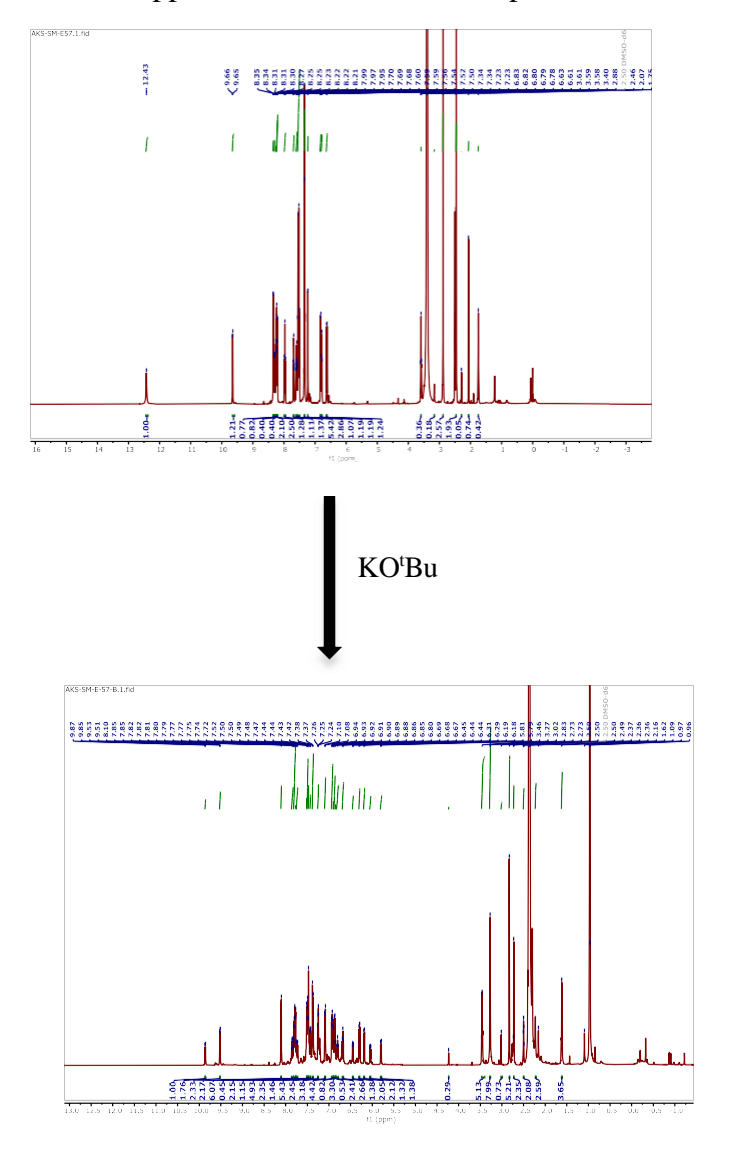


Fig. 50. ¹H NMR spectrum (500 MHz) of [**Ru-2**] in DMSO-d₆ after addition of base.

1.2 H₂ Bubbling:

In the same NMR J-Young NMR tube, after the disappearance of the proton peak, H₂ gas was introduced for 1–2 hours.

Observation: After analyzing the ¹H NMR spectrum, no hydride peak was observed in the shielded region, nor was any signal detected in the protic (deshielded) region.

This indicates that the Ru-2 catalyst is unable to split H₂ and is not suitable for H₂ splitting catalysis.

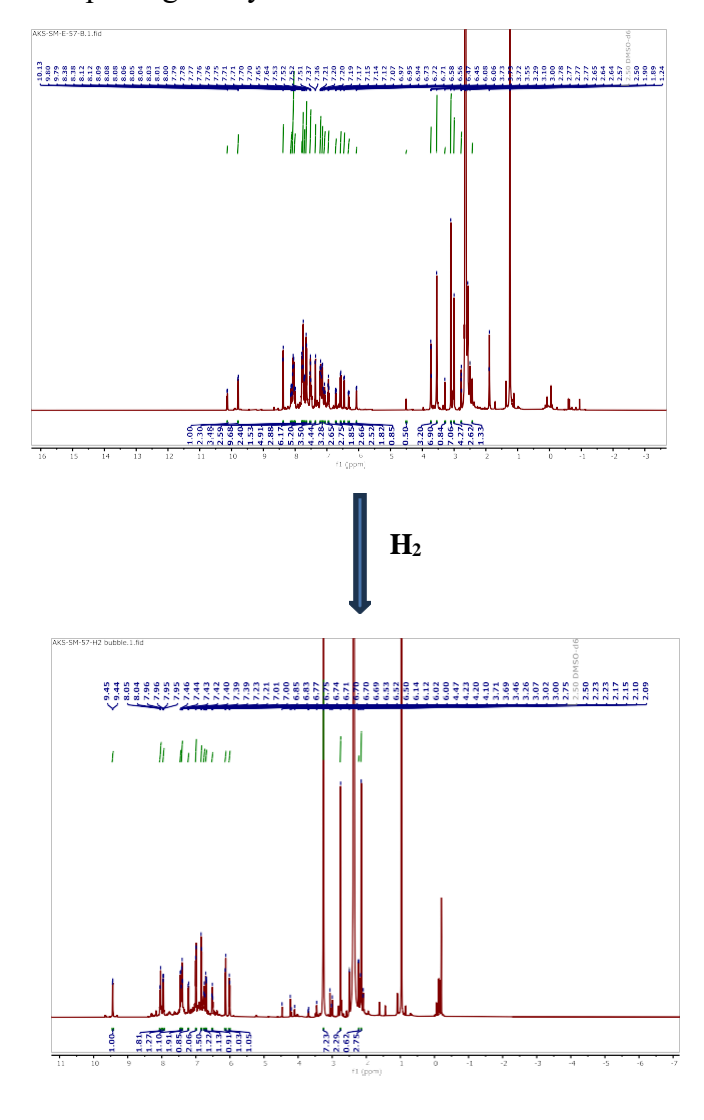


Fig. 51. ¹H NMR spectrum (500 MHz) of [**Ru-2**] in DMSO-d₆ after H₂ bubbling.

CHAPTER-4: CONCLUSION:

In conclusion, a series of phosphine-free Ru(II) complexes bearing protic NHC ligands, namely Ru-1 and Ru-2, were successfully synthesized. Both complexes were thoroughly characterized using liquid chromatography mass spectrometry (LC-MS), multinuclear NMR spectroscopy, and single-crystal X-ray diffraction, the latter of which confirmed the molecular structure of Ru-1. The catalytic performance of these Ru(II)-pNHC complexes was explored in various reactions, including amine double dehydrogenation, nitrile hydration, and water oxidation. Notably, Ru-2 was found to be inactive in H₂-splitting catalysis. Electrochemical studies revealed that the chloro-substituted complex acts as an efficient water oxidation catalyst, although it exhibits slightly different electrochemical behavior compared to its iodo analogue.

4.1 <u>Future Prospective:</u>

Further studies will focus on optimizing the reaction conditions for amine double dehydrogenation to achieve better conversions. Subsequent investigation of the substrate scope will provide insights into the versatility and limitations of the catalytic system. Additional catalytic reactions and electrochemical studies may provide deeper insights into the reactivity and potential applications of these Ru(II)-pNHC complexes.

4.2 REFERENCES:

- (1) Lupp, D.; Huang, K.-W. The Importance of Metal–Ligand Cooperativity in the Phosphorus–Nitrogen PN³ P Platform: A Computational Study on Mn-Catalyzed Pyrrole Synthesis. *Organometallics* **2020**, *39* (1), 18–24. https://doi.org/10.1021/acs.organomet.9b00102.
- (2) Soleilhavoup, M.; Bertrand, G. Cyclic (Alkyl)(Amino)Carbenes (CAACs): Stable Carbenes on the Rise. *Acc. Chem. Res.* **2015**, *48* (2), 256–266. https://doi.org/10.1021/ar5003494.
- (3) Yadav, D.; Misra, S.; Kumar, D.; Singh, S.; Singh, A. K. Cationic Ruthenium(II)–NHC Pincer Complexes: Synthesis, Characterisation and Catalytic Activity for Transfer Hydrogenation of Ketones. *Appl. Organomet. Chem.* **2021**, *35* (8), e6287. https://doi.org/10.1002/aoc.6287.
- (4) Younus, H. A.; Su, W.; Ahmad, N.; Chen, S.; Verpoort, F. Ruthenium Pincer Complexes: Synthesis and Catalytic Applications. *Adv. Synth. Catal.* 2015, 357 (2–3), 283–330. https://doi.org/10.1002/adsc.201400777.
- (5) Gandolfi, C.; Heckenroth, M.; Neels, A.; Laurenczy, G.; Albrecht, M. Chelating NHC Ruthenium(II) Complexes as Robust Homogeneous Hydrogenation Catalysts. *Organometallics* 2009, 28 (17), 5112–5121. https://doi.org/10.1021/om900356w.
- (6) Colacino, E.; Martinez, J.; Lamaty, F. Preparation of NHC– Ruthenium Complexes and Their Catalytic Activity in Metathesis Reaction. *Coord. Chem. Rev.* 2007, 251 (5–6), 726–764. https://doi.org/10.1016/j.ccr.2006.07.017.
- (7) Selective Catalysis for Renewable Feedstocks and Chemicals; Nicholas, K. M., Ed.; Topics in Current Chemistry; Springer International Publishing: Cham, 2014; Vol. 353. https://doi.org/10.1007/978-3-319-08654-5.

- (8) N-Heterocyclic Carbenes: From Laboratory Curiosities to Efficient Synthetic Tools, 2nd edition.; Díez-González, S., Ed.; RSC catalysis series; Royal Society of Chemistry: Cambridge, 2017. https://doi.org/10.1039/9781782626817.
- (9) Chakraborty, S.; Barik, S.; Biju, A. T. N-Heterocyclic Carbene (NHC) Organocatalysis: From Fundamentals to Frontiers. *Chem. Soc. Rev.* **2025**, *54* (3), 1102–1124. https://doi.org/10.1039/D4CS01179A.
- (10) Zhang, D.; Zi, G. N-Heterocyclic Carbene (NHC) Complexes of Group
 4 Transition Metals. *Chem. Soc. Rev.* 2015, 44 (7), 1898–1921.
 https://doi.org/10.1039/C4CS00441H.
- (11) Hopkinson, M. N.; Richter, C.; Schedler, M.; Glorius, F. An Overview of N-Heterocyclic Carbenes. *Nature* **2014**, *510* (7506), 485–496. https://doi.org/10.1038/nature13384.
- (12) Öfele, K. 1,3-Dimethyl-4-imidazolinyliden-(2)-pentacarbonylchrom ein neuer übergangsmetall-carben-komplex. *J. Organomet. Chem.* **1968**, *12* (3), P42–P43. https://doi.org/10.1016/S0022-328X(00)88691-X.
- (13) Wanzlick, H.-W.; Schönherr, H.-J. Direct Synthesis of a Mercury Salt-Carbene Complex. *Angew. Chem. Int. Ed. Engl.* **1968**, 7 (2), 141–142. https://doi.org/10.1002/anie.196801412.
- (14) Arduengo, A. J.; Harlow, R. L.; Kline, M. A Stable Crystalline Carbene. *J. Am. Chem. Soc.* **1991**, *113* (1), 361–363. https://doi.org/10.1021/ja00001a054.
- (15) Pan, C.; Ho, P.-Y.; Huang, W.-Q.; Huang, G.-F.; Zhang, L.-H.; Tritton, D. N.; Yiu, S.-M.; Man, W.-L.; Ko, C.-C.; Leung, C.-F.; Ni, W.-X. Transformable *Cis Trans* Isomerism of Ruthenium(II) Complexes with Photoactivated Anticancer Activity. *Inorg. Chem. Front.* 2025, 10.1039.D4QI02665A. https://doi.org/10.1039/D4QI02665A.
- (16) Donthireddy, S. N. R.; Mathoor Illam, P.; Rit, A. Ruthenium(II) Complexes of Heteroditopic N-Heterocyclic Carbene Ligands: Efficient Catalysts for C–N Bond Formation via a Hydrogen-Borrowing Strategy under Solvent-Free Conditions. *Inorg. Chem.* 2020, 59 (3), 1835–1847. https://doi.org/10.1021/acs.inorgchem.9b03049.

- (17) Ernst, J. B.; Muratsugu, S.; Wang, F.; Tada, M.; Glorius, F. Tunable Heterogeneous Catalysis: N-Heterocyclic Carbenes as Ligands for Supported Heterogeneous Ru/K-Al₂ O₃ Catalysts To Tune Reactivity and Selectivity. *J. Am. Chem. Soc.* **2016**, *138* (34), 10718–10721. https://doi.org/10.1021/jacs.6b03821.
- (18) Ceramella, J.; Troiano, R.; Iacopetta, D.; Mariconda, A.; Pellegrino, M.; Catalano, A.; Saturnino, C.; Aquaro, S.; Sinicropi, M. S.; Longo, P. Synthesis of Novel N-Heterocyclic Carbene-Ruthenium (II) Complexes, "Precious" Tools with Antibacterial, Anticancer and Antioxidant Properties. *Antibiotics* 2023, 12 (4), 693. https://doi.org/10.3390/antibiotics12040693.
- (19) Xie, P.; Guo, F. Molecular Design of Ruthenium Complexes for Dye-Sensitized Solar Cells Based on Nanocrystalline TiO2. *Curr. Org. Chem.* **2011**, *15* (22), 3849–3869. https://doi.org/10.2174/138527211797884539.
- (20) Jain, N.; Mary, A.; Singh, T.; Gadiyaram, S.; Jose, D. A.; Naziruddin, A. R. Heteroleptic Ruthenium(II) Complexes Featuring *N* -Heterocyclic Carbene-Based C^N Donor Sets for Solar Energy Conversion. *New J. Chem.* **2023**, *47* (28), 13476–13485. https://doi.org/10.1039/D3NJ01432K.
- (21) Younus, H. A.; Ahmad, N.; Su, W.; Verpoort, F. Ruthenium Pincer Complexes: Ligand Design and Complex Synthesis. *Coord. Chem. Rev.* 2014, 276, 112–152. https://doi.org/10.1016/j.ccr.2014.06.016.
- (22) Fogler, E.; Balaraman, E.; Ben-David, Y.; Leitus, G.; Shimon, L., J. W.; Milstein, D. New CNN-Type Ruthenium Pincer NHC Complexes. Mild, Efficient Catalytic Hydrogenation of Esters. *Organometallics* 2011, 30 (14), 3826–3833. https://doi.org/10.1021/om200367j.
- (23) Pattabiraman, V. R.; Bode, J. W. Rethinking Amide Bond Synthesis. *Nature* **2011**, *480* (7378), 471–479. https://doi.org/10.1038/nature10702.
- (24) Guo, B.; De Vries, J. G.; Otten, E. Hydration of Nitriles Using a Metal–Ligand Cooperative Ruthenium Pincer Catalyst. *Chem. Sci.*

- **2019**, 10 (45), 10647–10652. https://doi.org/10.1039/C9SC04624K.
- (25) Allen, C. L.; Williams, J. M. J. Metal-Catalysed Approaches to Amide Bond Formation. *Chem. Soc. Rev.* **2011**, *40* (7), 3405. https://doi.org/10.1039/c0cs00196a.
- (26) Ahmed, T. J.; Knapp, S. M. M.; Tyler, D. R. Frontiers in Catalytic Nitrile Hydration: Nitrile and Cyanohydrin Hydration Catalyzed by Homogeneous Organometallic Complexes. *Coord. Chem. Rev.* **2011**, *255* (7–8), 949–974. https://doi.org/10.1016/j.ccr.2010.08.018.
- (27) Tu, T.; Wang, Z.; Liu, Z.; Feng, X.; Wang, Q. Efficient and Practical Transition Metal-Free Catalytic Hydration of Organonitriles to Amides. *Green Chem.* **2012**, *14* (4), 921. https://doi.org/10.1039/c2gc16637b.
- (28) O'Connor, C. Acidic and Basic Amide Hydrolysis. *Q. Rev. Chem. Soc.* **1970**, *24* (4), 553. https://doi.org/10.1039/qr9702400553.
- (29) Marcé, P.; Lynch, J.; Blacker, A. J.; Williams, J. M. J. A Mild Hydration of Nitriles Catalysed by Copper(II) Acetate. *Chem. Commun.* **2016**, *52* (7), 1436–1438. https://doi.org/10.1039/C5CC08714G.
- (30) Tomás-Mendivil, E.; García-Álvarez, R.; Vidal, C.; Crochet, P.; Cadierno, V. Exploring Rhodium(I) Complexes [RhCl(COD)(PR₃)] (COD = 1,5-Cyclooctadiene) as Catalysts for Nitrile Hydration Reactions in Water: The Aminophosphines Make the Difference. *ACS Catal.* **2014**, *4* (6), 1901–1910. https://doi.org/10.1021/cs500241p.
- (31) Prejanò, M.; Alberto, M. E.; Russo, N.; Marino, T. Hydration of Aromatic Nitriles Catalyzed by Mn-OH Complexes: A Rationalization from Quantum Chemical Investigations. *Organometallics* **2020**, *39* (18), 3352–3361. https://doi.org/10.1021/acs.organomet.0c00436.
- (32) Yadav, S.; Gupta, R. Hydration of Nitriles Catalyzed by Ruthenium Complexes: Role of Dihydrogen Bonding Interactions in Promoting Base-Free Catalysis. *Inorg. Chem.* **2022**, *61* (39), 15463–15474. https://doi.org/10.1021/acs.inorgchem.2c02058.
- (33) Tomás-Mendivil, E.; Suárez, F. J.; Díez, J.; Cadierno, V. An Efficient Ruthenium (IV) Catalyst for the Selective Hydration of Nitriles to Amides in Water under Mild Conditions. *Chem. Commun.* **2014**, *50* (68), 9661. https://doi.org/10.1039/C4CC04058A.

- (34) A. Kleemann, J. Engel, B. Kutscher, D. Reichert, *Pharmaceutical Substance: Synthesis Patents, Applications, 4th Edn., Georg Thieme Verlag, Stuttgart, 2001.*
- (35) Fleming, F. F.; Yao, L.; Ravikumar, P. C.; Funk, L.; Shook, B. C. Nitrile-Containing Pharmaceuticals: Efficacious Roles of the Nitrile Pharmacophore. *J. Med. Chem.* **2010**, *53* (22), 7902–7917. https://doi.org/10.1021/jm100762r.
- (36) Fleming, F. F.; Yao, L.; Ravikumar, P. C.; Funk, L.; Shook, B. C. Nitrile-Containing Pharmaceuticals: Efficacious Roles of the Nitrile Pharmacophore. *J. Med. Chem.* **2010**, *53* (22), 7902–7917. https://doi.org/10.1021/jm100762r.
- (37) Teodori, E.; Dei, S.; Garnier-Suillerot, A.; Gualtieri, F.; Manetti, D.; Martelli, C.; Romanelli, M. N.; Scapecchi, S.; Sudwan, P.; Salerno, M. Exploratory Chemistry toward the Identification of a New Class of Multidrug Resistance Reverters Inspired by Pervilleine and Verapamil Models. *J. Med. Chem.* 2005, 48 (23), 7426–7436. https://doi.org/10.1021/jm050542x.
- (38) Hughes, C. A.; Robinson, L.; Tseng, A.; MacArthur, R. D. New Antiretroviral Drugs: A Review of the Efficacy, Safety, Pharmacokinetics, and Resistance Profile of Tipranavir, Darunavir, Etravirine, Rilpivirine, Maraviroc, and Raltegravir. *Expert Opin. Pharmacother.* **2009**, *10* (15), 2445–2466. https://doi.org/10.1517/14656560903176446.
- (39) Dutta, I.; Yadav, S.; Sarbajna, A.; De, S.; Hölscher, M.; Leitner, W.; Bera, J. K. Double Dehydrogenation of Primary Amines to Nitriles by a Ruthenium Complex Featuring Pyrazole Functionality. *J. Am. Chem. Soc.* **2018**, *140* (28), 8662–8666. https://doi.org/10.1021/jacs.8b05009.
- (40) Gunanathan, C.; Milstein, D. Applications of Acceptorless Dehydrogenation and Related Transformations in Chemical Synthesis. *Science* 2013, 341 (6143), 1229712. https://doi.org/10.1126/science.1229712.
- (41) Wang, Z.; Belli, J.; Jensen, C. M. Homogeneous Dehydrogenation of Liquid Organic Hydrogen Carriers Catalyzed by an Iridium PCP

- Complex. *Faraday Discuss.* **2011**, *151*, 297. https://doi.org/10.1039/c1fd00002k.
- (42) Bernskoetter, W. H.; Brookhart, M. Kinetics and Mechanism of Iridium-Catalyzed Dehydrogenation of Primary Amines to Nitriles. *Organometallics* 2008, 27 (9), 2036–2045. https://doi.org/10.1021/om701148t.
- (43) Kundu, A.; Barman, S. K.; Mandal, S. Dangling Carboxylic Group That Participates in O–O Bond Formation Reaction to Promote Water Oxidation Catalyzed by a Ruthenium Complex: Experimental Evidence of an Oxide Relay Pathway. *Inorg. Chem.* **2022**, *61* (3), 1426–1437. https://doi.org/10.1021/acs.inorgchem.1c03105.
- (44) Deng, X.; Tüysüz, H. Cobalt-Oxide-Based Materials as Water Oxidation Catalyst: Recent Progress and Challenges. *ACS Catal.* **2014**, *4* (10), 3701–3714. https://doi.org/10.1021/cs500713d.
- (45) Shatskiy, A.; Bardin, A. A.; Oschmann, M.; Matheu, R.; Benet-Buchholz, J.; Eriksson, L.; Kärkäs, M. D.; Johnston, E. V.; Gimbert-Suriñach, C.; Llobet, A.; Åkermark, B. Electrochemically Driven Water Oxidation by a Highly Active Ruthenium-Based Catalyst. *ChemSusChem* **2019**, *12* (10), 2251–2262. https://doi.org/10.1002/cssc.201900097.
- (46) Hisatomi, T.; Wang, Q.; Zhang, F.; Ardo, S.; Reisner, E.; Nishiyama, H.; Kudo, A.; Yamada, T.; Domen, K. Photocatalytic Water Splitting for Large-Scale Solar-to-Chemical Energy Conversion and Storage. *Front. Sci.* 2024, 2, 1411644. https://doi.org/10.3389/fsci.2024.1411644.
- (47) Singh, A. K.; Roy, L. Evolution in the Design of Water Oxidation Catalysts with Transition-Metals: A Perspective on Biological, Molecular, Supramolecular, and Hybrid Approaches. *ACS Omega* **2024**, *9* (9), 9886–9920. https://doi.org/10.1021/acsomega.3c07847.
- (48) Yang, J.; An, J.; Tong, L.; Long, B.; Fan, T.; Duan, L. Sulfur Coordination Effects on the Stability and Activity of a Ruthenium-Based Water Oxidation Catalyst. *Inorg. Chem.* **2019**, *58* (5), 3137–3144. https://doi.org/10.1021/acs.inorgchem.8b03199.

- (49) Gersten, S. W.; Samuels, G. J.; Meyer, T. J. Catalytic Oxidation of Water by an Oxo-Bridged Ruthenium Dimer. J. Am. Chem. Soc. 1982, 104 (14), 4029–4030. https://doi.org/10.1021/ja00378a053.
- (50) Zong, R.; Thummel, R. P. A New Family of Ru Complexes for Water Oxidation. J. Am. Chem. Soc. 2005, 127 (37), 12802–12803. https://doi.org/10.1021/ja054791m.
- (51) Yang, J.; Wang, L.; Zhan, S.; Zou, H.; Chen, H.; Ahlquist, M. S. G.; Duan, L.; Sun, L. From Ru-Bda to Ru-Bds: A Step Forward to Highly Efficient Molecular Water Oxidation Electrocatalysts under Acidic and Neutral Conditions. *Nat. Commun.* 2021, 12 (1), 373. https://doi.org/10.1038/s41467-020-20637-8.
- (52) Zhan, S.; De Gracia Triviño, J. A.; Ahlquist, M. S. G. The Carboxylate Ligand as an Oxide Relay in Catalytic Water Oxidation. *J. Am. Chem. Soc.* **2019**, *141* (26), 10247–10252. https://doi.org/10.1021/jacs.9b02585.
- (53) Duan, L.; Bozoglian, F.; Mandal, S.; Stewart, B.; Privalov, T.; Llobet, A.; Sun, L. A Molecular Ruthenium Catalyst with Water-Oxidation Activity Comparable to That of Photosystem II. *Nat. Chem.* **2012**, *4* (5), 418–423. https://doi.org/10.1038/nchem.1301.
- (54) Heravi, M. M.; Kheilkordi, Z.; Zadsirjan, V.; Heydari, M.; Malmir, M. Buchwald-Hartwig Reaction: An Overview. *J. Organomet. Chem.* 2018, 861, 17–104. https://doi.org/10.1016/j.jorganchem.2018.02.023.
- (55) Wang, L.; Liu, N.; Dai, B.; Hu, H. Selective C–N Bond-Forming Reaction of 2,6-Dibromopyridine with Amines. *Eur. J. Org. Chem.* 2014, 2014 (29), 6493–6500. https://doi.org/10.1002/ejoc.201402619.